PLOS Computational Biology

RESEARCH ARTICLE

Biologically-constrained spiking neural network for neuromodulation in locomotor recovery after spinal cord injury

Raymond Chia*, Chin-Teng Lin

Computational Intelligence and Brain Computer Interfaces Lab, School of Computer Science, Faculty of Engineering and Information Technology, University Technology Sydney, Sydney, New South Wales, Australia

* raymond.chia@uts.edu.au

OPEN ACCESS

Citation: Chia R, Lin C-T (2026) Biologically-constrained spiking neural network for neuromodulation in locomotor recovery after spinal cord injury. PLoS Comput Biol 22(1): e1013866. https://doi.org/10.1371/journal.pcbi.1013866

Editor: Mark Alber, University of California Riverside, UNITED STATES OF AMERICA

Received: January 6, 2025

Accepted: December 22, 2025

Published: January 6, 2026

Peer Review History: PLOS recognizes the benefits of transparency in the peer review process; therefore, we enable the publication of all of the content of peer review and author responses alongside final, published articles. The editorial history of this article is available here: https://doi.org/10.1371/journal.pcbi.1013866

Abstract

Presynaptic inhibition after spinal cord injury (SCI) has been hypothesised to disproportionately affect flexion reflex loops in locomotor spinal circuitry. Reducing gamma-aminobutyric acid (GABA) inhibitory activity increases the excitation of flexion circuits, restoring muscle activation and stepping ability. Conversely, nociceptive sensitisation and muscular spasticity can emerge from insufficient GABAergic inhibition. To investigate the effects of neuromodulation and proprioceptive sensory afferents in the spinal cord, a biologically constrained spiking neural network (SNN) was developed. The network describes the ankle flexor motoneuron (MN) reflex loop with inputs from ipsilateral Ia- and II-fibres and tonically firing interneurons. The model was tuned to a Baseline level of locomotive activity before simulating an inhibitory-dominant and body-weight supported (BWS) SCI state. Electrical stimulation (ES) and serotonergic agonists were simulated by the excitation of dorsal fibres and reduced conductance in excitatory neurons. ES was applied across all afferent fibres without phase- or muscle-specific protocols. The present computational findings suggest that reducing stance-phase GABAergic inhibition on flexor motoneurons could facilitate more physiological flexor activation during locomotion. The model further predicts that neuromodulatory therapy, together with body-weight support, modulates the balance of synaptic excitation and inhibition in ankle flexor motoneurons to mitigate excessive inhibitory drive in the ankle flexor circuitry.

Author summary

SCI is a life-altering condition that often leaves young adults paralysed and reliant on others for support. Restoring the ability to walk is a critical goal to help improve independence and quality of life for people living with SCI. Promising new treatments, such as spinal cord stimulation and drug therapies, aim to reawaken the neurons that control walking. However, scientists still do not entirely understand

Data availability statement: All relevant data are within the manuscript and its Supporting information files.The experiment code can be found at https://github.com/rchia16/balancing-locomotor-networks.git.

Funding: This work was supported by a Research Training Program (RTP) Scholarship provided by the Australian Government and awarded to R.C for the period 2017–2022 to support the completion of his doctoral degree. The funders had no role in study design, data collection and analysis, decision to publish, or preparation of the manuscript. R.C received a stipend salary from the Australian Government under the Research Training Program during this period.

Competing interests: The authors have declared that no competing interests exist.

how these treatments work. In this study, we developed a detailed computer model of the neural circuits involved in walking to test how therapies such as serotonin-boosting drugs, ES, and BWS training might help. Our findings suggest that these treatments can work together to reduce excessive inhibition that blocks ankle movement, leading to smoother and more coordinated steps. This research helps uncover how these therapies work and provides insights to develop better rehabilitation strategies for improving walking after SCI.

Introduction

SCI globally affects an estimated 9 million people as of 2019, with an age standardised incident rate of about 109 per 100,000 [1]. In the event of SCI, damage to the nervous tissue can result in loss of voluntary control, sensation, spasticity, diaphragm dysfunction, pressure ulcers, and pain syndromes [2,3]. Sufferers of SCI often report non-physical symptoms such as emotional disorders, loss of independence, depression, anxiety, and clinical levels of stress [4]. The lifelong management places an intense financial burden not only on the patients and their communities, but also on the broader economic landscape [5,6]. Lifetime medical costs in Canada can range from $1.47 to $3 million CAD (2013 prices) per person [7], £1.12 million per person in the UK (2016 prices) [8], and range from $0.77 to $1.3 million USD (1995 prices) in the US [9]. Recovering voluntary muscle activity and returning locomotion activity to SCI sufferers could save societal and patient costs while also improving the patient's quality of life [10,11].

Recovering gait remains a top priority for people living with SCI [12]. Flexor activity is critical for step progression during locomotion, acting as a shock absorber before foot strike [13], adapting step-height to continue locomotion progression [14], and resetting locomotion [15]. Increasing the excitability of locomotor networks after paralysis can improve locomotor capabilities; however, hyperexcitation of flexor muscles can result in spastic muscle expression, leading to poor balance and coordination [16–18]. Maintaining an excitation-inhibition balance of excitability emerges as an intuitive solution to enabling robust locomotor expression.

SCI interrupts normal bidirectional signalling, leading to dysfunctional neural circuitry, tilting the balance of excitation and inhibition [19]. Lack of descending activity keeps MNs at a predominantly inhibited state, while inhibitory populations in the dorsal and intermediate zone become over-reactive [20,21]. A large percentage of the SCI population experience spastic muscle activity, likely due to insufficient release of GABA neurotransmitters [22–26]. Nevertheless, even with an overly excited or inhibited environment and detached from brain inputs, the locomotor spinal circuit can continue to express coordinated motor function given sufficient excitation and contextually relevant sensory information [27–31].

Proprioception is a critical sensory input to entrain and recover locomotion after SCI [32–34]. Proprioceptive afferent innervation is widespread and diverse, projecting to MNs [35–37], GABAergic [38,39], and serotonergic [40–43] interneurons (INs) in the dorsal and intermediate zone of the spinal cord. Long and short axons spread

across multiple segments and are organised spatially and by modality [37,44–46]. Proprioceptive interneurons (PINs) are mainly excitatory, most inhibitory populations projecting ipsilaterally [47]. Due to their complex and integratory nature, PINs have been suggested to be a possible neural detour around spinal lesions, recovering voluntary sensorimotor control after SCI [46,48–51].

Genetic labelling of spinal cord interneurons has identified V2a interneurons (Chx10$^+$) as a crucial population for coordinating left/right coordination [52] and locomotor speeds [53,54]. V2a interneurons reside in laminae VII and receive serotonergic, glutamatergic inputs from the brainstem and sensory inputs from dI5 INs and mechanosensory feedback [53,55–58]. V2a interneurons locally project bursting glutamatergic excitation to ipsilateral V0 interneurons and MNs [55,59,60]. Moreover, ablation of V2a interneurons has been shown to prevent the recovery of suprathreshold ES facilitated locomotion recovery [61]. Therefore, inclusion of the V2a population in the present model allowed us to investigate how neuromodulation and sensory feedback influence excitatory drive and recovery of flexor motor function after injury.

After SCI, axons spared from injury allow voluntary activation and sensation of the body past lesion sites [51,62]. Traditional rehabilitation therapy leverages these residual connections to maximise motor skills via therapeutic exercise or overcome losses with assistive devices [28,63]. Neuromodulation techniques such as spinal cord ES [30,31,64,65] and pharmacology [51,66,67] have shown to recover locomotor activity after SCI. Moreover, chronic application of ES in conjunction with physical rehabilitation enabled volitional muscle activation even without ES [29]. Although these observations show promise for new and effective neurorehabilitation therapies, the mechanisms of action and synergy between sensory ensembles and ES remain in question [68,69].

It is natural to seek methods to return excitation to sub-lesional networks after losing descending input [70]. Most ES techniques have sought to excite and entrain locomotion by activating dorsal roots in the epidural space [69,71–74]. However, ES, in the same anatomical space, can also evoke inhibition and restore balance to an overly excited network [23,24,75]. A more in-depth and nuanced view of ES therapy is required to fully appreciate the complexity of modulating the neural environments. A key question remains: How do neuromodulation therapies integrate with sensory information? We hypothesise that spinal cord locomotor circuits require balanced excitation and inhibition to coordinate flexor activity.

Understanding excitation and inhibition balance experimentally remains challenging due to the complexity of interacting neural pathways. Computational modelling offers a complementary method to test how specific neural architectures and synaptic mechanisms contribute to locomotor activity.

Computational models have been central in linking neural architecture to locomotor output. Studies of commissural and long propriospinal interneurons have helped elucidate how propriospinal circuits stabilise gait across speeds [76]. Building on these frameworks, combining modelling and experimental approaches has revealed the role of V3 neurons in speed-dependent left-right interlimb coordination [77].

These models feature detailed architectures but often rely on reciprocally inhibiting phase oscillators [78,79] driven by tonic inputs that mimic descending mesencephalic locomotor region activity [80–82]. While suitable for neurologically intact systems, such assumptions break down after SCI, where the supraspinal drive is reduced or absent, although sub-lesional afferents remain intact.

To address this limitation, several studies have integrated peripheral feedback into spinal locomotor circuits, yielding physiologically grounded spiking models and enabling the design of novel neuromodulation therapies [69,71,74,83]. A bio-inspired controller combining a balance controller, a central pattern generator (CPG), and a sensory feedback network reproduced human gait kinematics and ground reaction forces by optimising for effort and stability [83]. Similarly, by combining spiking networks with finite element modelling, scientists were able to experimentally converge model outputs to rodent ES results, revealing activation sites and recruitment dynamics [71]. Incorporating locomotion-specific afferents into these models further enabled the development of function-specific ES therapies [69] and clarified interactions between suprathreshold ES and proprioceptive afferents [74].

Iterative refinements of CPG-based frameworks have expanded our understanding of locomotor control and informed new therapeutic strategies. However, the current spinal locomotor network modelling landscape omits presynaptic inhibition.

This study aims to understand the effect of SCI-induced imbalanced presynaptic inhibition in sensory-driven rodent locomotor spinal networks. We describe a biologically constrained tibialis anterior (TA) SNN rodent model receiving heterogeneous excitatory and inhibitory synapses, including GABAergic presynaptic inhibition. A combination of ES and serotonin agonist (5-HT) neuromodulators are simulated in an SCI and SCI with BWS locomotion setting. We show that combining BWS with ES reduces overactive stance-evoked GABA inhibition and returns TA MN firing rates towards Baseline.

Methods

A biologically constrained SNN was developed to investigate neuromodulation effects on sensory-driven rodent spinal locomotor circuits. Simulations were run on an Intel Xeon Gold 6238R 2.2GHz Processor. The software was developed in Python 3.10.0 using the Brian2 neural simulator module (v2.6.0) [84]. The simulation time step was set to 50 μs and Euler approximations for ordinary differential equation solving. A total of eight locomotor steps were simulated, where gait stance and swing phases were split at 65% of the gait cycle [85]. This study simulated three different neurological environments, including a Baseline, SCI, and SCI with a BWS state. Each neurological state was modulated with inputs from ES and 5-HT. The Baseline state was set by validating the static outputs of the SNN model against previously validated computational data and experimental observations in healthy rodents. SCI condition was set by increasing the paired synapses between GABA INs and TA MNs by a factor of 1.6, as experimentally reported in previous rodent SCI studies [86]. Finally, the BWS state was defined as the scalar reduction of Ia and II afferent firing rates as reported from treadmill BWS experiments recording EMG [87].

The SNN model architecture was biologically constrained using synaptic connections inferred from previous cell staining [39,71,86,88], electrophysiological [53,89–94], and genetic works [55,95–99]. A second biological constraint was set by matching neuron cell dynamics to experimentally measured electrophysiological neural recordings [53,55,74,88,95,97,100–102]. Specific parameter settings are described in the sections below and set to be within biologically plausible ranges. Parameter definitions have been summarised in Table 1. Finally, propriosensory inputs were constrained to previously validated musculoskeletal and muscle spindle models [74].

Simulated data were first tested for normality using the Shapiro-Wilk test, where $p > 0.05$ indicated that the data did not significantly deviate from a normal distribution. Normally distributed data were compared using a paired t-test, while non-normal data were analysed using the Wilcoxon signed-rank test. Distributions were considered significantly different if $p < 0.05$

Equivalence between groups was assessed using pairwise two one-sided tests (TOST) at an $\alpha_{equiv} = 0.05$ level (95% CI). The null hypothesis of non-equivalence was rejected if both one-sided tests were significant ($p_{equiv} < 0.05$), indicating that the mean difference lay within the predefined equivalence region (± 15 Hz). The region of practical equivalence (ROPE) for comparisons between conditions was defined as half the minimal detected burst rate for TA motoneurons in rodents at rest (30 –60 Hz) [103]. Within-timestep differences were tested for significance using within-step permutation testing with 2000 repetitions.

The experiment code can be found at https://github.com/rchia16/balancing-locomotor-networks.git.

Afferent signal inputs

Ia and II TA and gastrocnemius medialis (GM) muscle afferent signals were calculated by using musculoskeletal and muscle spindle models during locomotion. The signals were retrieved from the publicly accessible GitHub repository associated with the original publication [74]. To emulate BWS afferent signals, both TA and GM Ia and II data were offset by a

Table 1. List of definitions relevant to the description of the SNN model.

Parameter	Definition
N	Number of axons/neurons
τ_{mem}	Membrane time constant
τ_{ref}	Refractory period
τ_{γ}	GABA spillover time constant
V	Membrane potential
E_l	Reverse potential
V_{th}	Threshold potential
V_{reset}	Membrane potential after spike
C_m	Membrane capacitance
r_{axon}	Axon radius
l	Length
g_L	Leak conductance
I	Input current from noise or synapses
w	Adaptation variable
τ_w	Adaptation variable time constant
Δ_V	Sharpness of action potential initiation
a	Voltage coupling parameter
b	Spike triggered adaptation value
p_{syn}	Synaptic connection probability

https://doi.org/10.1371/journal.pcbi.1013866.t001

scalar amount using values from electrophysiological experiments [87]. The new BWS equations were set to Eq (1) where $K_{GM} = -0.6$ and $K_{TA} = -0.122$, scaling the EMG envelope to 40% and 87.8% respectively, simulating 60% effective body weight. This corresponds to an effective reduction in Ia and II afferent firing rates of approximately 60% of GM muscle afferents and 12.2% for TA muscle afferents, consistent with experimentally observed muscle-specific reductions in EMG amplitude under 60% BWS [87].

EMG was adapted from past computational studies and calculated as per S2 Algorithm [74]. The equations refer to $x_{stretch}$ as stretch, $v_{stretch}$ as stretch velocity, and EMG_{env} as the min-max normalised EMG envelope [104]. Since EMG_{env} magnitude ranged between 0 and 1, a scalar offset can be applied to the afferent signal inputs [74]. Afferent signals were set as timed array Poisson-distributed inputs with a sampling frequency of 200 Hz, and connected to leaky integrate and fire (LIF) axon models, see Eq 3 and Fig 1A and 1B. Parameters were set according to previously validated computational models [71] and tuned to replicate the input firing rate, see Table 2 and Table 5. Background noise of afferent axons (I_{noise}) was modelled as a normally distributed variable with a standard deviation scaled to 0.3 pA. Tuning was validated with Pearson correlation coefficient and the mean absolute error. For detailed results, refer to S1 Table in the Supplementary Information. For a complete algorithmic description of a LIF model, see S1 Algorithm.

$$\text{Ia firing rate} = 50 + 2x_{stretch} + 4.3 \cdot sign(v_{stretch}) \cdot |v_{stretch}|^{0.6} + K \cdot 50 \cdot EMG_{env} \quad (1)$$

$$\text{II firing rate} = 80 + 13.5x_{stretch} + K \cdot 20 \cdot EMG_{env} \quad (2)$$

$$\frac{dV}{dt} = \frac{E_l - V}{\tau} + \frac{I_{noise}}{C_m \cdot \pi r_a l} \quad (3)$$

Spiking neural network

The SNN model simulated the ipsilateral rodent ankle flexor's mono- and di-synaptic stretch and stretch velocity afferent reflexes. Proprioceptive afferents innervated the TA MN, GABA, Ia inhibitory, and V2a interneurons [107,108]. Ia inhibitory interneurons (IaINs) receiving Ia and II afferent inputs of the flexor and extensor muscles were reciprocally inhibited [96]. GABA INs applied presynaptic inhibition to excitatory inputs of the TA MN [86,109]. V2a INs received flexor II

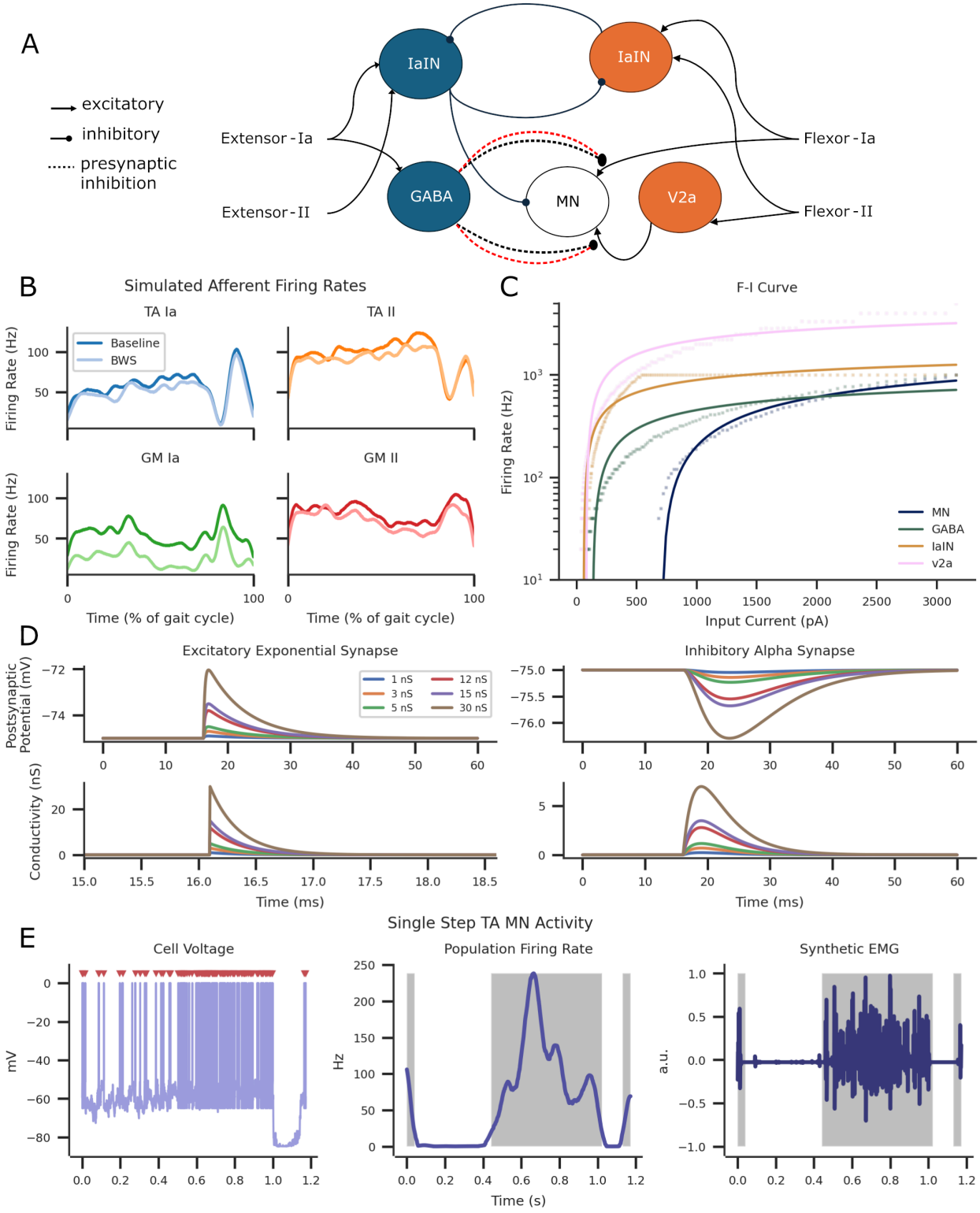

Fig 1. Computational SNN model of the flexor network with GM extensor and TA flexor proprioceptive Ia and II inputs. (A) Biologically constrained SNN ankle flexor model. Arrow ends indicate excitation, circle ends indicate inhibition, and dotted line with circle ends indicate presynaptic inhibition connections. The red dotted lines represent an increased number of SCI-induced GABA synapses. (B) Afferent axon firing rates for extensor (GM) and flexor (TA) Ia- and II-fibres in the Baseline and BWS condition. (C) Frequency-Current (F-I) curve for each neuron simulated in the SNN

model. Each point reflects a single data point for the injected current and the solid lines were fitted using a logarithmic function. Input current was applied with a 200 ms pulse width from a stimulus range of 10 to 3160 pA. (D) Excitatory exponential synapses and inhibitory alpha synapses across different conductances. (E) Simulated TA MN output from a single step. Left illustrates the MN membrane potential activity with spiking activity indicated with red triangles. The firing rates were converted into 25 ms window widths and smoothened with a Gaussian filter (middle). Synthetic EMG activity was generated from recorded spiking activity by convolving Gaussian wavelets (right). Grey shading highlights detected bursts of firing rate activity.

https://doi.org/10.1371/journal.pcbi.1013866.g001

Table 2. Afferent axon parameters for LIF model, including references for each value where relevant.

Axon Parameter	Value	Reference
N	60	[69]
τ	30 ms	[69]
τ_{ref}	1.6 ms	[69]
E_l	−80 mV	[71]
V_{th}	−60 mV	[105]
V_{reset}	−70 mV	[105]
C_m	1.0 μF/cm^2	[106]
r_{Ia}	9 ±0.2 μm	[71]
r_{II}	4.4 ±0.5 μm	[71]
$l^{\dagger}$	1 mm	-

† Assumed variable, held constant throughout tuning.

https://doi.org/10.1371/journal.pcbi.1013866.t002

afferent inputs and applied tonic excitation to TA MNs [55,59]. TA MNs received monosynaptic excitation from flexor Ia afferents [98,110]. Refer to Fig 1A for an illustration of the entire network and Fig 1C for frequency-current (F-I) response using 200 ms pulse widths across a stimulus range of 10 to 3160 pA. For a visual example of tonic spiking neural firing, refer to S2 and S3 Figs.

IaINs were modelled as conductance-based LIF neurons receiving excitation from Ia and II afferent fibres and inhibition from opposing IaINs, see Eq 4. I_{syn} is the cumulative synaptic current from excitatory and inhibitory components. IaIN parameters in Table 3 were set to match experimental results [74,88].

$$\frac{dV}{dt} = \frac{g_L(E_L - V) + I_{syn}}{C_m} \tag{4}$$

Table 3. Ia inhibitory, GABA, V2a IN and MN parameters. Parameter values were set based on results recorded in experiments or other validated computational studies.

Parameter	IaIN	GABA	V2a	MN
N	196 [74]	196†	196 [74]	169 [69]
C_m	31.1 pF [88]	100 pF‡	45 pF [55]	162 pF [111]
E_L	−70 mV [88]	−70 mV†	−53 mV [55]	−75 mV [71,97]
V_{th}	−50 mV†	−50 mV†	−42 mV [55]	−50 mV [111]
V_{reset}	−65 mV [88]	−62.3 mV†	−47 mV [55]	−65 mV‡
g_L	5 nS [88]	1.2 nS‡	1.2 nS [55]	27 nS [112]
Δ_v	–	2 mV‡	0.5 mV‡	0.05 mV‡
a	–	2 nS‡	2 nS‡	–
τ_w	–	20 ms [97]	55 ms [55]	–

†Assumed variables, held constant during tuning
‡Tuned parameters, adjusted during model calibration.

https://doi.org/10.1371/journal.pcbi.1013866.t003

GABA presynaptic inhibitory INs and V2a INs were modelled as conductance-based adaptive exponential (AdEx) LIFs [101]. GABA parameters [97] and V2a parameters [53,55,95] were set as per experimental results. AdEx equations were defined as per Eqs (5) and (6). GABA and V2a IN parameters were set per Table 3.

$$\frac{dV}{dt} = \frac{g_L(E_L - V) + g_L(\Delta_V \exp\frac{V-V_{th}}{\Delta_V}) + I_{syn} - w}{C_m} \tag{5}$$

$$\frac{dw}{dt} = \frac{a(V - E_L) - w}{\tau_w} \tag{6}$$

TA flexor MNs were modelled as exponential LIFs receiving excitation from TA Ia fibres, V2a INs, inhibition from GM originating IaINs and presynaptic inhibition from GABA INs [38,58,74]. The equation for TA MNs was the same as Eqs (5) and (6) where $w = 0$. Parameters in Table 3 were set to best estimate experimental results [88,111,112]. MN responses under varying stimulation pulse widths are shown in S2 Fig.

To capture the net excitability increase produced by 5-HT agonists, we used a single-parameter surrogate at the motoneuron: a reduction of the leak conductance (g_L). This mirrors prior network models that emulate 5-HT with a single conductance change (e.g. 40% reduction of K(Ca)) to reproduce persistent inward current mediated plateaus and enhanced recruitment [69,113]. Consistent with these precedents, MN and V2a IN g_L was reduced by 40% under $SCI_{5\text{-HT}}$ and $SCI_{5\text{-HT+ES}}$ conditions and by 15% under $BWS_{5\text{-HT}}$ and $BWS_{5\text{-HT+ES}}$, reflecting the modulated serotonergic activity after 5-HT administration. Decreasing the leak conductance increases membrane resistance and neuronal excitability, thus simulating the modulatory effects of 5-HT on spinal circuits.

Synapses

Alpha and exponential conductance synapses were used to describe inhibitory and excitatory synapses, respectively, see Table 4 and Fig 1D. The reversal potential of excitatory synapses was set to 0 mV, while inhibitory synapses were set to −75 mV [69]. This was to ensure the hyperpolarisation without instability. II-fibre synapse weights were scaled by a factor of 0.33 to simulate the effect of smaller axon size [74,114].

Synaptic connections, with the exclusion of GABA, were determined by probabilities specified in Table 5. Axon synapses included a 2±0.3 ms delay accounting for diameter variability [115]. GABA connections to TA MNs were predetermined by index rules dependent on the experiment condition. Synaptic connections between GABA and TA MN indexes were joined together if their absolute index difference was less than 4, see S1 Fig. GABA connections were tuned to qualitatively match the population firing profile of previously reported simulations using the same dataset [69,74]. SCI condition GABA connections were increased by 160% as seen in flexor MNs after SCI transection, simulating an inhibitory-dominant environment [86].

Presynaptic inhibition was a multiplicative gain, scaling synaptic weights of each excitatory connection to the TA MN population [91,97,116,117]. GABA spillover was modelled as a linear decrease in release factor, γ, see Eq (7). λ determined the strength of the inhibition and set to a value of 0.4. C_{GABA} was considered a unitless value for local GABA

Table 4. Alpha and exponential synapse and GABA spillover parameters. Alpha synapses were used for inhibitory connections while exponential synapses were used for excitatory connections.

Synapse Parameter	Value	Reference
τ_{exc}	0.25 ms	[74]
$\tau_{inh,rise}$	2 ms	[74]
$\tau_{inh,decay}$	4.5 ms	[74]
τ_{γ}	20 ms	[97]

https://doi.org/10.1371/journal.pcbi.1013866.t004

Table 5. Synapse connection probabilities (p_{syn}) and synaptic conductance by source and target neurons. Excitatory (exc.) and inhibitory (inh.) synaptic conductance applies to target neurons. All values in this table were tuned to reproduce afferent signals and keep stability during afferent driven locomotion.

Source	Target	p_{syn}	Exc.	Inh.
Axon	IaIN	0.3	7 nS	–
Axon	GABA	0.4	12 nS	–
Axon	V2a	0.6	1 nS	–
$IaIN_{TA/GM}$	$IaIN_{TA/GM}$	0.1	–	3 nS
Axon, V2a, IaIN	MN	0.3	30 nS	10 nS

https://doi.org/10.1371/journal.pcbi.1013866.t005

concentration [118].

$$\tau_\gamma \frac{d\gamma}{dt} = -\gamma + \max(0, \min(1 - \lambda \cdot C_{GABA}, 1)) \tag{7}$$

Poisson distributed stimulus inputs were used to simulate subthreshold ES at a frequency of 40 Hz, amplitude of 10 mV, and pulse width of 0.2 ms, consistent with experimental protocols for locomotor facilitation [119–121]. This assumption is supported by previous studies demonstrating that exogenous excitatory drives can be represented as asynchronous Poisson inputs in cortical structures [122,123]. Each stimulation input was connected to three non-overlapping afferent fibres.

Photostimulation paradigms provide an experimentally controlled and reproducible framework for precise activation of neuronal populations under static and well-defined stimulation conditions [124,125]. Recent work has demonstrated that recurrent networks fitted to electrophysiological data can fail to predict responses to optogenetic perturbations, indicating incorrect underlying circuit mechanisms, whereas biologically grounded SNNs generalise more reliably to unseen optogenetic perturbations [126]. This establishes photostimulation as a principled means for validating the causal mechanisms implemented in SNN models.

To our knowledge, no validated SNN models have explicitly included presynaptic GABAergic inhibition in a controlled manner. Given that photostimulation responses provide an appropriate benchmark for assessing simulated effects. Therefore, we evaluated GABA interaction by testing if the model reproduced physiologically consistent firing patterns. This was done across random initialisations and beyond non-perturbed conditions.

Validation of GABAergic interactions was performed by adopting electrophysiological evoked-response experiments from intracellular recordings of the TA MN [97]. To simulate photostimulation of GABA neurons, a threshold current pulse was injected using the same pulse durations (1 ms), frequencies (50 Hz), and delays (45 ms) reported in the experimental protocol [97].

To validate the SNN model, an EMG signal (Fig 1E) was generated by convolving representative motor unit action potentials (S2 Algorithm), using the same parameters as experimental and previously validated computational models [69,74,127]. Population firing rates were averaged with a 25 ms Gaussian window for smoothening.

Bayesian modelling for seed equivalence

Given the random nature of the synaptic connections and background noise, the eight-step simulations were repeated across 32 random seeds. Repeating simulations across random seeds was performed to ensure the parameters were not overfit to a singular random seed and to improve the robustness of the study. To test for overfitting in the Baseline condition, equivalence testing across all seeds was performed with Bayesian inference modelling. Conditional and seed-dependent testing was completed using Bayesian hierarchical Linear Mixed Models (LMMs).

Temporal resolution was reduced by calculating mean firing rates for each step, and time (x-axis) was rescaled to [0,1] and expanded with a cubic B-spline bases $\beta(t_i)$. A spline for time and seed-specific random effects, nested within conditions, was fitted as per Eq (8). Let y_i be the output for observation i from seed $s(i)$ in condition $c(i)$ at step t_i.

$$\begin{aligned} y_i &= a_{c(i)} + a_{s(i)} + B(t_i)^\top \beta_{c(i)} + B(t_i)^\top \beta_{s(i)} + \epsilon_i \\ \epsilon_i &\sim \mathcal{N}(0,\, 5) \end{aligned} \tag{8}$$

In this equation, a_c represents the condition-level intercept and $B^\top \beta_c$ is the shared condition-level temporal trajectory. Seed effects were nested within condition and written in a non-centred parameterisation. We used weakly informed information priors $a_c \sim \mathcal{N}(0,\, 10)$, $\beta_c \sim \mathcal{N}(0,\, 2I)$, $\sigma_{LMM} \sim \mathit{HalfNormal}(2)$, and $\tau_{a,c}, \tau_{\beta,c} \sim \mathit{HalfNormal}(1)$. Posterior inference was performed with No-U-Turn Sampler (NUTS) method in PyMC [128,129]. Spline degree-of-freedom was set to 3, and the number of spline knots was set to 4. Regression was computed to minimise the root mean square between observations and model outputs. LMMs were considered well fit if no divergences were detected, all Gelman-Rubin statistics (chain convergence) were within the threshold ($\hat{R} < 1.05$), and posterior predictive fit reached threshold ($R^2 > 0.7$) [130].

$$\begin{aligned} a_s &= z_{a,s}\tau_{a,c(s)}, \quad z_{a,s} \sim \mathcal{N}(0,\, 1) \\ \beta_s &= z_{\beta,s}\tau_{\beta,c(s)}, \quad z_{\beta,s} \sim \mathcal{N}(0,\, I_p) \end{aligned} \tag{9}$$

We considered the SNN model to be equivalent across seeds if, at an intercept level $P(\tau_{a,c} < \epsilon_{int}) \geq 0.9$, and at a dynamics level, $P(\tau_{\beta,c} < \epsilon_{dyn}) \geq 0.9$. The ROPE for both LMM intercepts was defined as ϵ_{int} = 5 Hz. This was calculated as 16.67% of the minimum recorded TA firing rate (30 Hz) during quiet resting activity [131] and standard deviations seen in locomotor activity experimentally recorded in rodents [132]. The ROPE for dynamic trajectory was defined as $\epsilon_{dyn} = \max(5,\, 0.05 \max(y_c(t)))$, scaling with the fitted maximum rate amplitude. A 5 Hz floor was included to avoid vanishing thresholds in low-amplitude conditions, matching the relative temporal dynamics recorded during locomotion [131,133]. By setting a low TA firing rate during quiet resting activity in healthy rodents, we can more confidently assess seed
equivalence across conditions.

To avoid artificially inflating the effective sample size in subsequent statistical analyses, condition-dependent data were aggregated by averaging across all seeds within each step for a given condition. For inter-step analyses, each step's state was inherently dependent on the preceding states and their corresponding seed configurations; therefore, inter-step data were computed independently within each seed to preserve their dependency structure. Outliers were removed by using a z-score threshold of 3 standard deviations from the mean.

Results

Bayesian hierarchical statistical modelling was applied to fit the nested data structure for equivalence analysis across 32 random seed initialisations and eight steps. To ensure reliable inference, model fit was first assessed by comparing the observed and model-predicted firing rate distributions. Posterior predictive checks showed strong agreement between observed and predicted values, indicating a satisfactory model fit. Although the model underestimated the exponential behaviour near zero firing rates, see Fig 2B.

Model convergence and sampling stability were confirmed through multiple diagnostics. The posterior sampling energy diagnostic density plot demonstrated close agreement between the transition and marginal energy densities, indicating well-mixed chains (Fig 2B). Convergence diagnostics further supported stable sampling, with Gelman-Rubin statistics ($\hat{R} \leq 1.01$) and Bayesian fraction of missing information (BFMI >0.9) within acceptable ranges across all chains, see S2 Table.

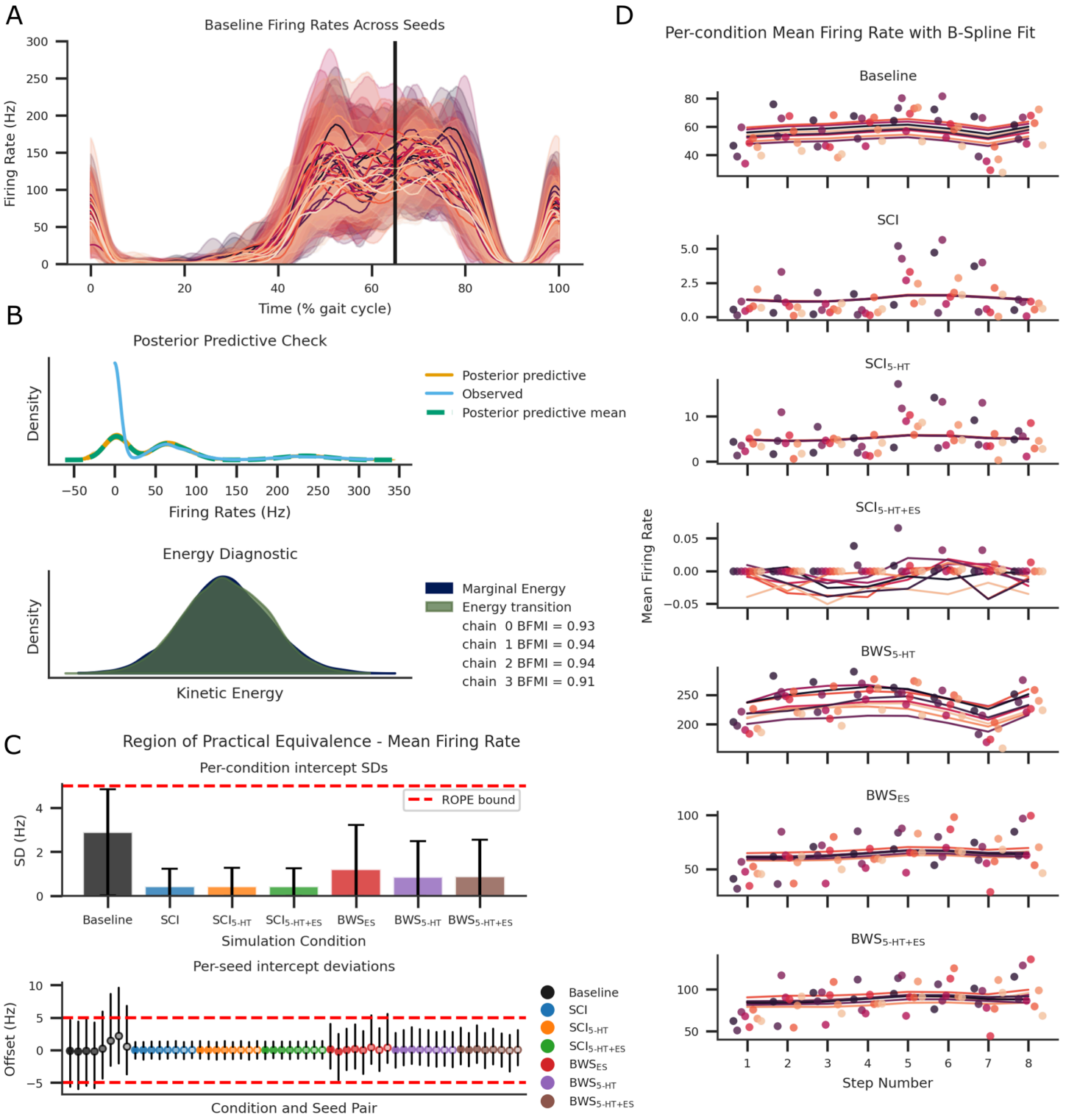

Fig 2. Step trials (n_{steps} = 8) were repeatedly simulated using 32 unique random seed value initialisations. Recorded TA MN cell spiking events were used to verify model equivalence across all random seeds. (A) The mean population firing rate and standard deviation of TA MNs across the step trials were calculated for each seed, represented by each colour. (B) The upper plot shows the posterior predictive check. Overlap between observed and model-predicted firing-rate densities indicates good model fit. The lower plot illustrates the energy diagnostic of Markov Chain Monte Carlo sampling. The close overlap between marginal and transition energies indicates stable sampling behaviour for the fitted LMM. (C) The posterior

standard deviation (SD) of seed-level intercept deviations within each condition are shown in the bar plot. These are further differentiated within the lower scatter plot as seed-specific intercept deviations. (D) Individual mean firing rates per step are plotted as individual markers. The fitted B-Spline LMM for each seed are colour matched line plots. Sub-figures (C) and (D) only plot eight seeds per condition to avoid overpopulating the figure.

https://doi.org/10.1371/journal.pcbi.1013866.g002

Together, these results confirm that the hierarchical LMM converged robustly and provides a reliable basis for statistical inference. Seed-level intercepts and seed-specific deviations were contained within the ROPE, see Fig 2C. Additional results on seed equivalence across steps and conditions are presented in S3 Table. In summary, aggregating temporal firing rates to mean values per seed and step produced well-converged models that demonstrate equivalence across conditions.

To complement this statistical validation, a spinal reflex recruitment protocol was implemented to verify the physiological plausibility of interactions between neural populations, synapses, and stimulation inputs within the SNN framework. Early- (ER), middle- (MR), and late-response (LR) latencies were defined as 1 ms, 4 ms, and 7 ms respectively [133]. The protocol was adapted from previous animal and simulation experiments and qualitatively assessed model behaviour under static conditions [69,134]. Afferent fibre and direct motoneuron recruitment data, retrieved from validated computational models [74], were coupled with identical stimulation profiles [71]. Electrical pulses of 0.5 ms were applied with an interstimulus interval of 1 s, with stimulus amplitudes ranging from 20 to 600 μA, encompassing the parameters (100 –300 μA) shown experimentally to facilitate locomotion in rats [66,134].

The SNN model described in the methods section does not couple spatial distances or electrode geometry. To match the acquired recruitment data, the minimal required stimulus required to elicit a spike was determined for each neuron and applied to the binary matrix encoding neuron index over time. As shown in Fig 3A, increasing stimulation intensities progressively recruited efferent fibres and suppressed MR and LR amplitudes, consistent with previously reported simulations and in vivo recordings [69,74,134]. Although simulated EMG amplitudes lack physiological scaling, the relative shape, latency, and modulation of evoked responses closely matched experimental [134] and validated computational data [69,71], supporting the model's biological realism.

Additionally, GABA interaction validation was performed by adopting electrophysiological evoked response experiments in EPSP recordings of the TA MN (Fig 3B). The ratios of EPSPs during control and photostimulation conditions were within range of experimental results ($0.5 < EPSP_{\lambda}/EPSP < 0.8$) [97].

The SNN model was further verified within a dynamic setting (Fig 3C) using previously simulated afferent fibre firing rate profiles during locomotion [74]. MN firing rates were processed with the same window size (4 ms) used in rodent experiments and validated by comparing TA MN burst firing rates and periods during locomotion [103,135]. The simulated burst activity during locomotion fell within the experimentally reported ranges for burst firing rates (100 –500 Hz) [103] and burst period (0.5 –0.9 s) [135], supporting the model's ability to reproduce physiologically realistic locomotor dynamics.

Having established the model's validity under dynamic conditions, we next examined how network activity evolved across Baseline and SCI simulations averaged over multiple steps. During Baseline stepping, most variation occurred during the swing phase and at the transition between the swing and stance phases of the gait cycle, see Fig 4A. The TA MN population firing rates between Baseline and SCI conditions were significantly different across time (Fig 5A). Deterministically scaling the number of GABAergic synapses onto flexor MNs by 160% increased GABA scaling factor, γ, which reduced seed-aggregated mean firing rates by a factor of 50 and increased the coefficient of variation by a factor of 3.8, see Fig 4B and Table 6.

Simulated TA MN expression during the Baseline step cycles was attenuated with stimulation voltages greater than 20 mV and by stimulation frequencies greater than 60 Hz, refer to Fig 4C and 4D. Though, GABA and V2a INs firing rates were scaled according to stimulation frequency. While seed variation was less noticeable in interneurons, the TA MN saw a large variation during frequency sweeps greater than 60 Hz during stance to swing transition and swing periods.

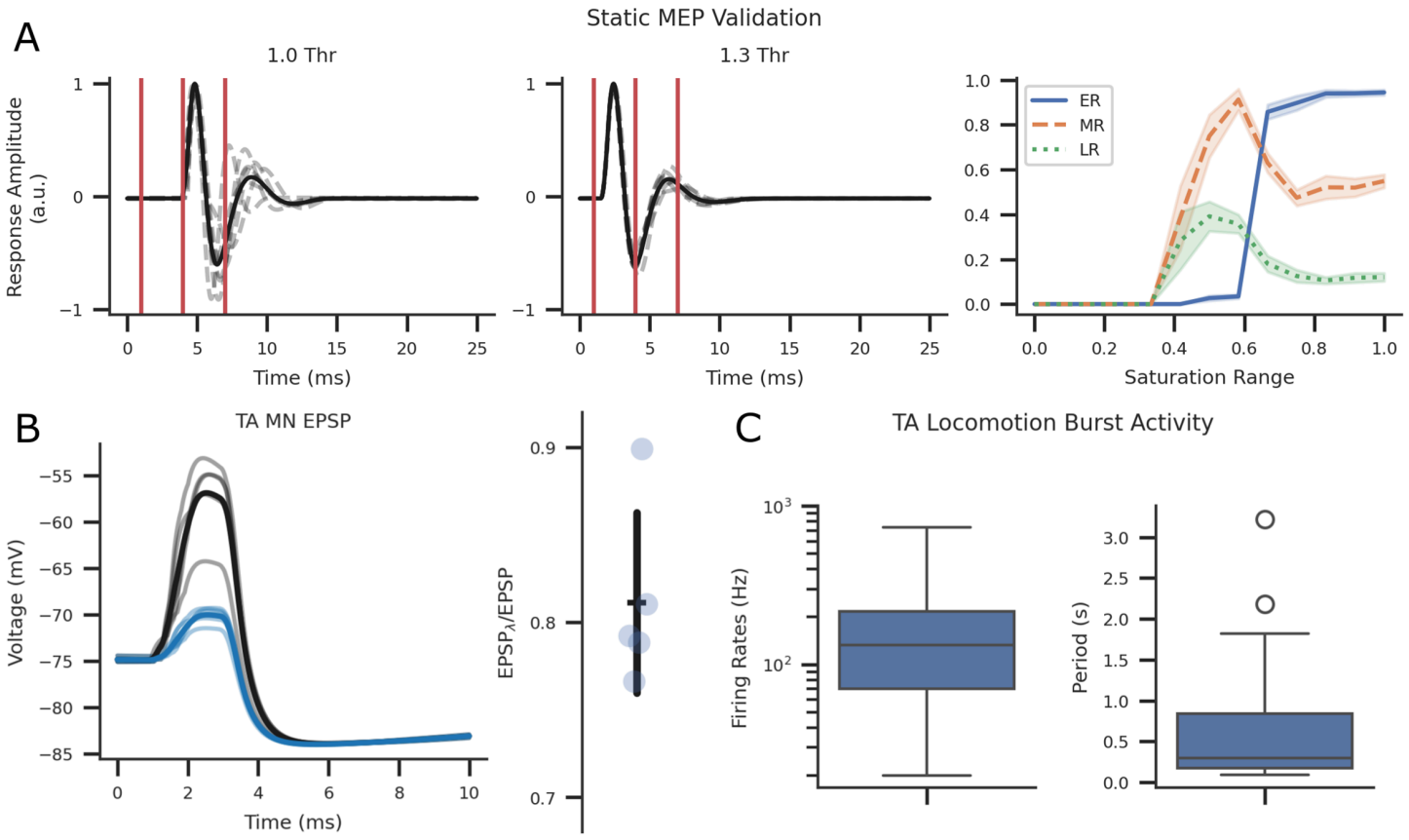

Fig 3. Static (n = 7) and dynamic (n = 9) qualitative and quantitative validation of the SNN model. (A) Motor evoked potentials (MEPs) at stimulation intensities ranging from 0-600 μA and 0.5 ms pulse width with 1 s between each pulse [69,134]. Results qualitatively match reported findings. (B) Modulation of excitatory post-synaptic potential in control (black trace) and GABA IN stimulation (blue trace) experiments. Transparent traces display seed specific trials, and opaque lines indicate the average across seeds. Fifteen 1 ms pulses at 50 Hz with a 45 ms delay stimulated GABA INs before delivering afferent fibre stimulation at 1.1x threshold [97]. The ratios between the photostimulated and control peaks were within the range of experimental results (0.4-0.9). (C) TA burst firing rates and periods during Baseline locomotion were within the range of experimental results [103,135].

https://doi.org/10.1371/journal.pcbi.1013866.g003

Statistical analysis on flexor activity after outlier removal during each phase presented a non-normal distribution in the swing and stance phases ($p < 0.05$). Swing phase flexor activity significantly differed between all simulated conditions, with the exclusion of Baseline-BWS_{ES} only. Stance phase flexor activity was significantly different in all simulated conditions. See Fig 5A and 5D for TA MN activity distributions in both swing and stance phases. Practical equivalence testing using an equivalence boundary of ±15 Hz, performed with TOST procedure on firing rate data, revealed equivalence between Baseline-BWS_{ES} pairs during stance phase (see Fig 5D and S4 Table).

Comparison of firing rate differences between the stance and swing phases, where stance was positive and swing was negative, showed significant differences in all Baseline pairs except for Baseline and $BWS_{5\text{-}HT+ES}$ condition (see Fig 5A and 5C). The same pattern was reflected in TOST equivalence tests (see Fig 5D and S4 Table.).

Pearson's correlation coefficient was calculated after aggregating the firing rate by averaging across seeds for each condition, see S4 Fig. Pairwise comparison of the Baseline condition with all other simulations found the highest correlation with BWS_{ES}, although only weakly correlated ($r = 0.11$; $p < 0.0001$).

While the GABA IN firing rates were the same between the simulated Baseline and SCI settings, increased GABAergic connections resulted in more frequent presynaptic inhibition activity on TA MN populations, see Figs 4B, 5A, and 5B.

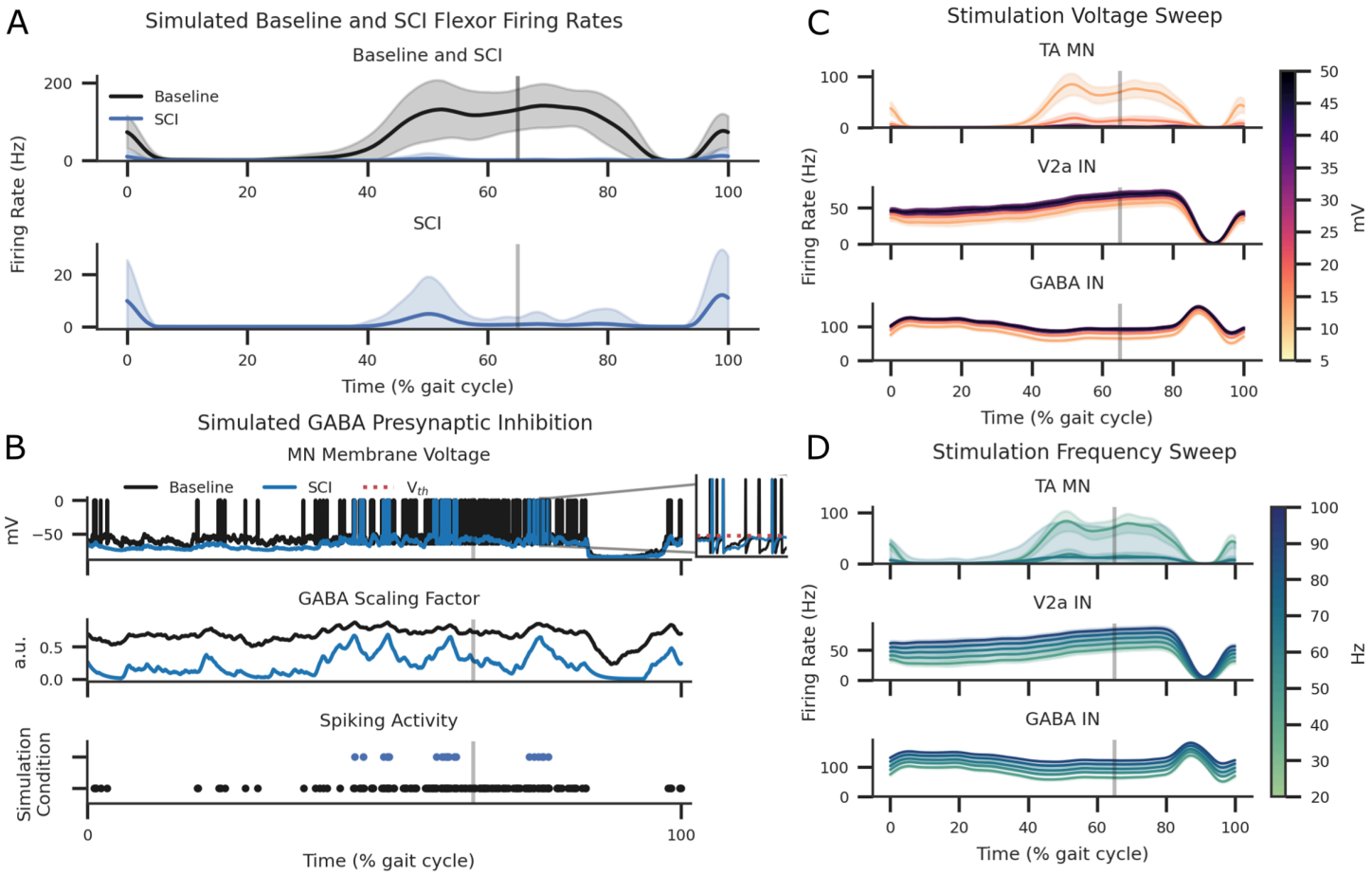

Fig 4. The effect of increased GABA synapses and excessive stance induced inhibition on TA MNs in addition to the effect of ES stimulation voltage and frequency on the Baseline condition stepping across each neuron are shown. Shaded areas represent standard deviations across seeds. (A) Average and standard deviation plots of eight steps during Baseline and simulated SCI conditions. The vertical grey line separates the stance (left of the grey line) and the swing (right of the grey line) phases, estimated at 65% of the gait cycle [85]. (B) SCI simulation of a single motoneuron receiving presynaptic inhibition by local concentration of GABA transmitters during a single step. Increased GABA scaling factor reduced the number of spike events near TA MN threshold. All shaded areas are standard deviations across seeds. (C) ES stimulation intensity sweep applied at 5, 10, 20, 30, 40, and 50 mV at a 40 Hz frequency. (D) ES stimulation frequency sweep applied at 20, 40, 60, 80, and 100 Hz at 10 mV amplitude. All ES was simulated with Poisson inputs to all flexor and extensor afferent axons.

https://doi.org/10.1371/journal.pcbi.1013866.g004

GABA IN firing rates were increased while receiving ES inputs (S5 Fig and S5 Table). V2a IN firing rates were equal between Baseline and SCI since it did not receive GABA IN synapses (S6 Fig and S5 Table). Simulating SCI serotonergic agonist activity by reducing the leak conductance of V2a INs significantly increased the V2a firing rates (S6 Fig), though this only slightly increased firing rates in MNs by a factor of 1.4 (S5 Table). This facilitatory effect was abolished when combined with ES, see Figs 6, 5A, and 5C. Without BWS, 5-HT application significantly increased V2a interneuron firing rates ($p < 0.0001$; Figs S6 and 6) but did not restore TA motoneuron activity to Baseline levels (Fig 5A and 5C). The facilitatory effects of 5-HT on TA motoneurons and V2a interneurons were abolished when ES was applied, coinciding with increased GABA interneuron activity (S5 Fig and S5 Table). Combining 5-HT with ES in the absence of BWS further reduced motoneuron excitation below that observed in the SCI condition.

BWS locomotion with SCI increased overall flexor activity to averages greater than the Baseline condition (Fig 5A, 5C, and 5D and Table 6). This was further amplified with the introduction of 5-HT. Applying ES without 5-HT smoothened

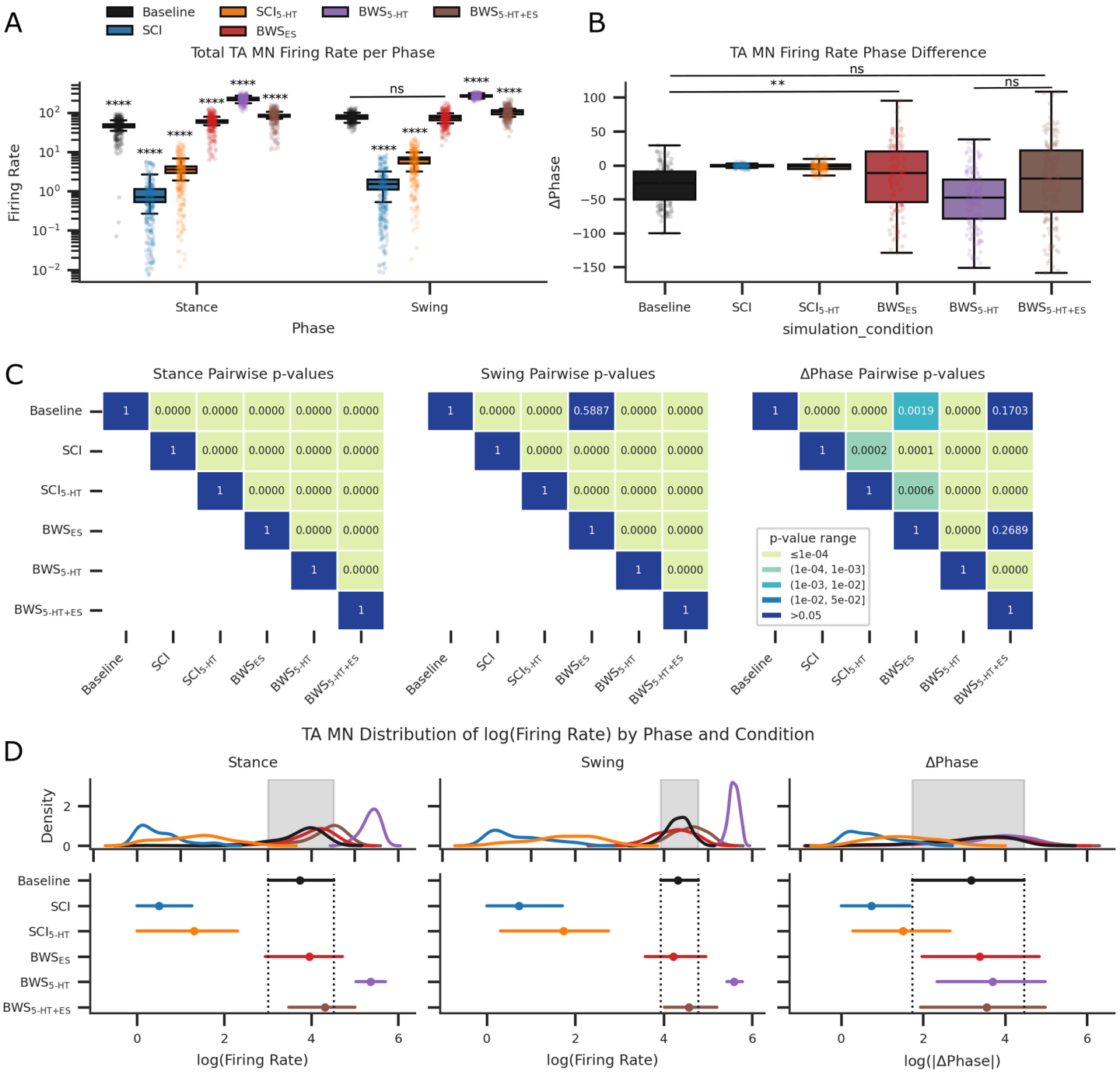

Fig 5. **Box-and-whisker plots with overlaid scatter data points for each step at each seed across conditions.** (A) Box-and-whisker plots were averaged over all seeds, yielding eight step datapoints and overlayed with scatter points for each phase. All swing and stance flexor activity was non-normal and significantly different with the exception of Baseline to BWS_{ES} during swing phase after paired t-tests. (B) Plots the overlayed box-and-whisker plot and scatter points for the phase difference between stance and swing. No statistical difference was detected in the mean firing rate phase differences between SCI and $SCI_{5\text{-}HT}$. (C) Displays the heatmap p-values for pairwise t-tests. (D) Plots the kernel density estimate to visualise the distribution of log-transformed observations for phases and their difference. TOST testing on log-transformed data resulted in no meaningful difference between Baseline and BWS_{ES} condition for both stance and swing phase. All TOST for phase difference calculations returned meaningfully large differences across all conditions.

https://doi.org/10.1371/journal.pcbi.1013866.g005

Table 6. Statistical calculations of seed-aggregated, phase-specific firing rates across experimental conditions for TA MN following z-score based outlier removal (values exceeding ±3 standard deviations). Reported results include mean, standard deviation (SD), and kurtosis for each locomotor phase (stance and swing) and their difference.

Phase	Simulation Condition	Mean	SD	Kurtosis
Stance	Baseline	46.69	19.89	-0.50
	SCI	0.91	1.24	4.73
	$SCI_{5\text{-}HT}$	3.81	3.57	1.92
	BWS_{ES}	59.08	26.91	-0.41
	$BWS_{5\text{-}HT}$	218.41	44.93	-0.34
	$BWS_{5\text{-}HT+ES}$	81.81	32.67	-0.39
Swing	Baseline	76.96	19.75	-0.14
	SCI	1.57	1.91	2.01
	$SCI_{5\text{-}HT}$	6.26	4.81	0.48
	BWS_{ES}	73.90	32.01	-0.03
	$BWS_{5\text{-}HT}$	267.45	30.13	-0.31
	$BWS_{5\text{-}HT+ES}$	103.13	38.64	-0.14
ΔPhase	Baseline	-29.88	26.49	-0.68
	SCI	-0.73	2.14	1.81
	$SCI_{5\text{-}HT}$	-2.65	5.98	0.74
	BWS_{ES}	-16.15	48.74	-0.51
	$BWS_{5\text{-}HT}$	-50.84	42.49	-0.47
	$BWS_{5\text{-}HT+ES}$	-22.85	59.04	-0.50

https://doi.org/10.1371/journal.pcbi.1013866.t006

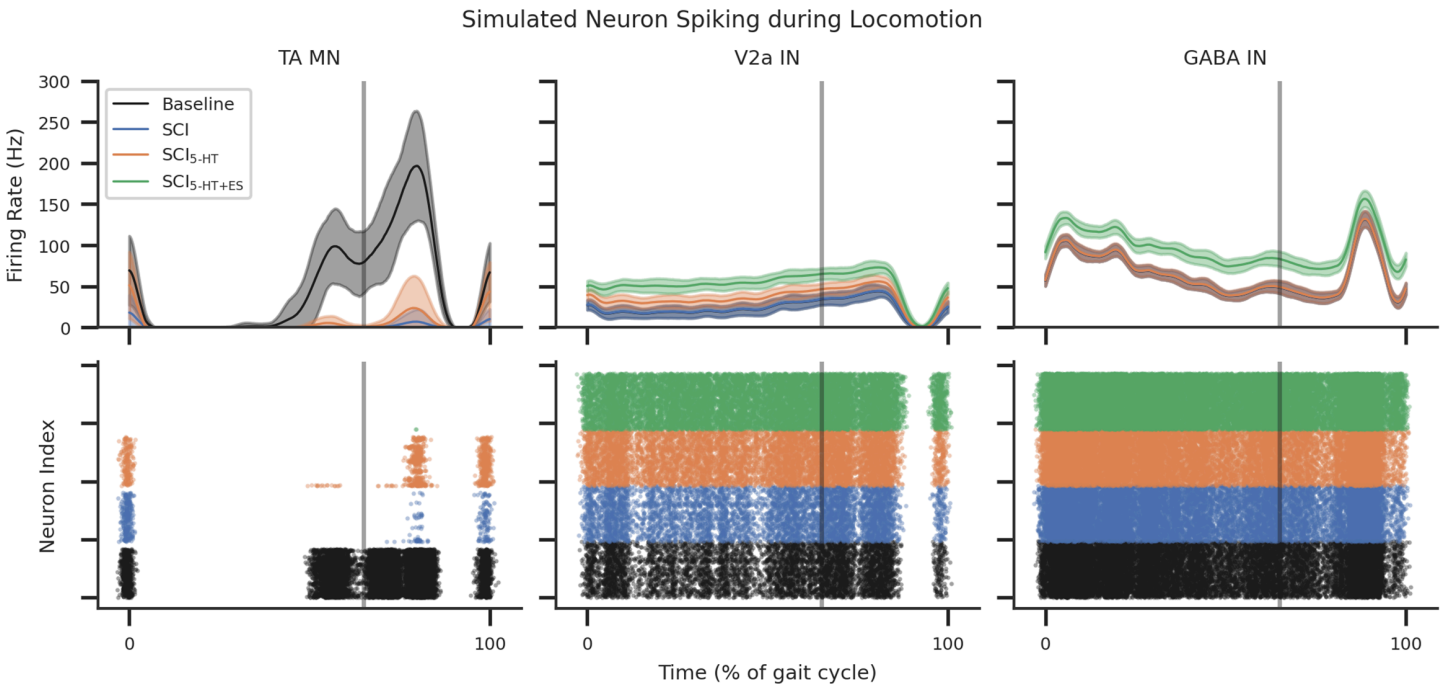

Fig 6. MN, V2a IN, and GABA IN firing rates during an example step, averaged over 32 seeds and shaded SD. The effect of SCI and SCI while receiving serotonergic agonists, (5-HT), and the combination of 5-HT and ES (5-HT+ES) were compared. The top row illustrates the population firing rates, and the bottom row shows the neuron population spike activity during the gait cycle.

https://doi.org/10.1371/journal.pcbi.1013866.g006

the output of MN activity, returning MN activations to Baseline. Combining 5-HT and ES further increased peak activity during the swing phase and reduced activations during stance phases, see Figs 7, 5A, and 5C. By re-introducing ES the

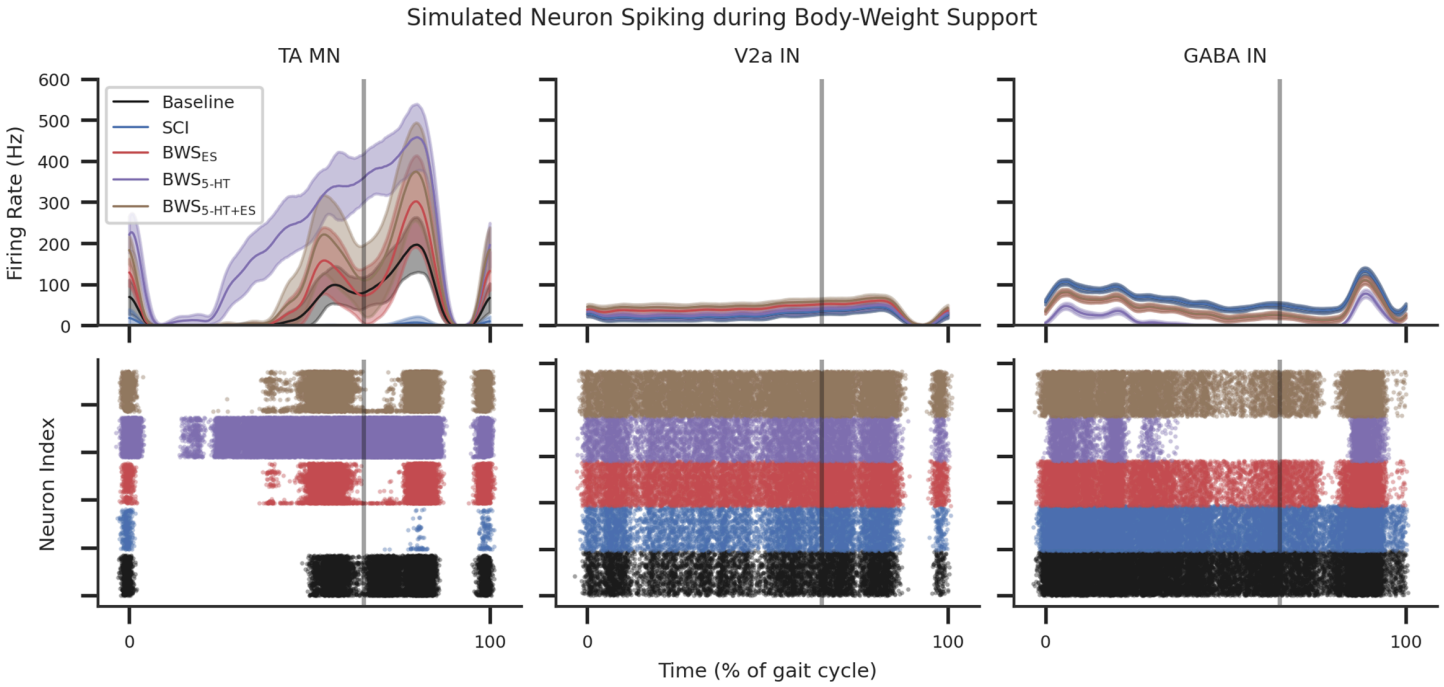

Fig 7. MN, V2a IN, and GABA IN firing rates during an example step during simulated BWS locomotion averaged over 32 seeds and shaded SD. The effect of BWS while receiving serotonergic agonists (5-HT) and the combination of 5-HT and ES (5-HT+ES) were compared. The top row illustrates the population firing rates and the bottom row shows the neuron population spike activity during the gait cycle.

https://doi.org/10.1371/journal.pcbi.1013866.g007

$BWS_{5\text{-HT}}$ condition, the inter-step differences in firing rate area under the curve (AUC) became statistically insignificant between BWS_{ES} and $BWS_{5\text{-HT+ES}}$ Fig 8D.

The reduction in flexor afferents during BWS decreased 5-HT modulated V2a IN activity towards SCI levels, though this effect did not reach statistical significance (S6 Fig and S5 Table). These changes were reversed under ES modulation. GABA IN activity was reduced in response to diminished stance-phase EMG during BWS Fig 7. Introducing ES restored GABA IN activity toward Baseline levels. GABA activity remained equivalent between BWS_{ES} and $BWS_{5\text{-HT+ES}}$ as 5-HT did not provide additional modulation; refer to Figs 7 and S5.

To further quantify how these neuromodulatory conditions affected the temporal dynamics of locomotion, inter-step differences were analysed across the Baseline and BWS_{ES} conditions by comparing firing rate, Fano factor (coefficient of variation), and AUC (Fig 8B, 8C, 8D, and Table 7). Permutation testing showed the greatest similarity in firing rates during active bursting periods in both stance and swing phases, whereas the Fano factor similarity was highest during quiescent periods (Fig 8B). A relative t-test revealed that 62.5% of stepwise AUC values differed significantly between Baseline and BWS_{ES}, compared with only 25% of Fano factor measurements, see Fig 8C and Table 8.

No significant AUC differences were found between Baseline and BWS_{ES} or between BWS_{ES} and $BWS_{5\text{-HT+ES}}$. Despite comparable firing rate profiles, TA MN spike-train variability differed between Baseline and BWS_{ES} during active spiking periods (see Figs 5C, 5D, and 8).

Discussion

A biologically constrained SNN model of the flexor reflex circuit was developed to investigate the integrative mechanisms between sensory and neuromodulation inputs to the spinal cord. Analysis of the stance and swing phases across eight steps under SCI conditions revealed serotonergic agonists re-excited V2a INs and TA MNs after SCI. Nonspecific ES

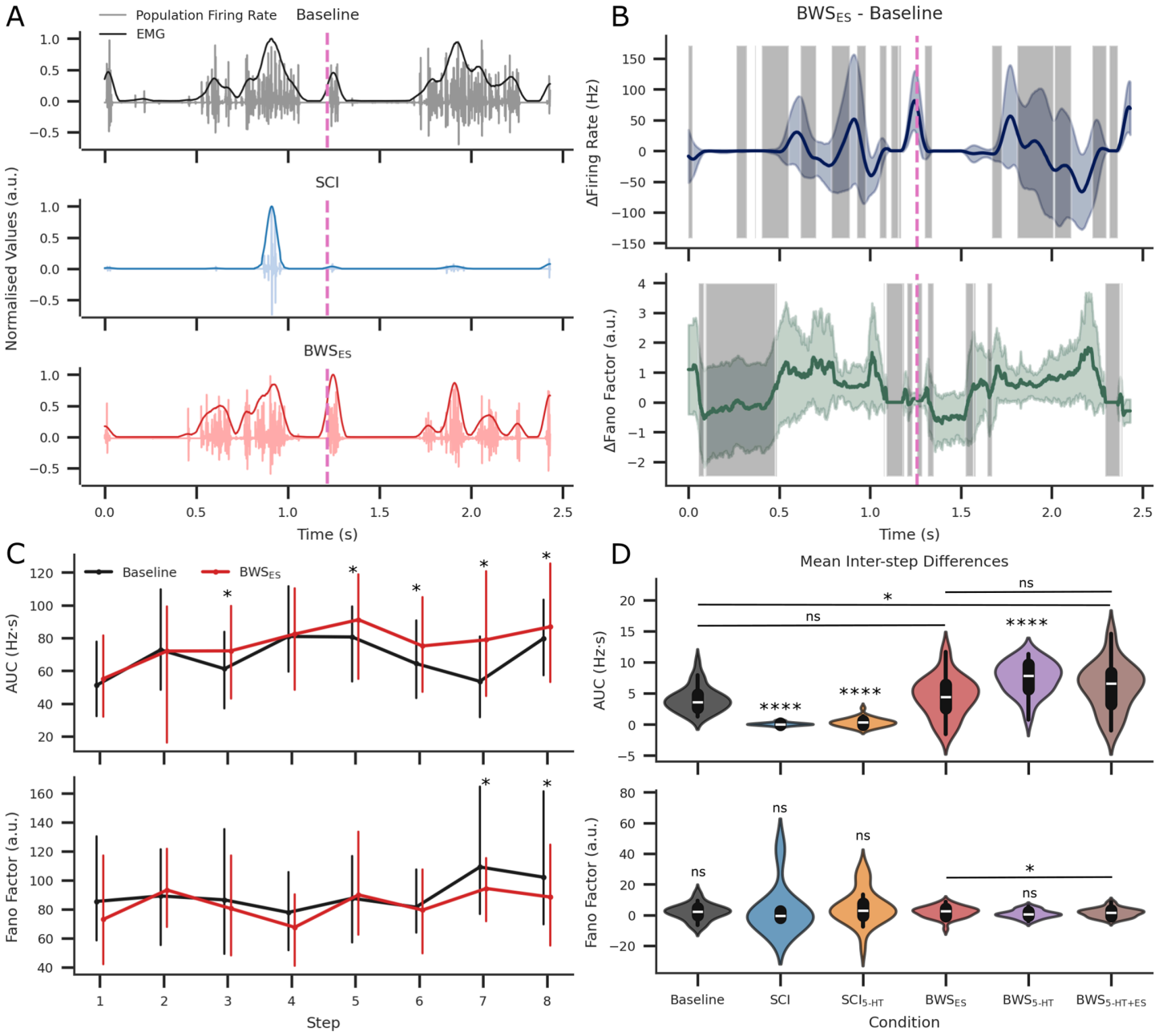

Fig 8. Using the population firing rates across steps and seeds, Area Under Curve (AUC) and Fano factors were calculated after downsampling by a factor of 10. (A) Population firing rates and EMG simulations for the Baseline, SCI, and BWS$_{ES}$ conditions. The pink vertical dashed line indicates the end of the first step and the beginning of the next. All y-axis values were normalised for easier viewing. (B) The firing rate and Fano factor difference between the Baseline and BWS$_{ES}$ conditions are plotted for the same step intervals as (A). Shaded in grey are areas that are not statistically significant after hierarchical permutation testing within each step ($p > 0.05$). (C) The step-by-step AUC and Fano factor with seed-aggregated means and highest density interval are plotted for the Baseline (black), SCI (blue), and BWS$_{ES}$ (red) conditions. (D) Inter-step differences in AUC and Fano factor were calculated for each seed and condition, providing a dependent sample size of 32. Conditional differences were pairwise t-tested and pairs with significance are shown. Baseline and BWS$_{ES}$ showed no significant difference in AUC. However, Baseline and BWS$_{ES}$ was significantly different when tested using the inter-step Fano factor.

https://doi.org/10.1371/journal.pcbi.1013866.g008

Table 7. Grand mean and standard deviation results of interstep differences aggregated over seeds for AUC and fano factor in the TA MN. Some steps did not return any spikes and so were not included in calculation for fano-factor.

	Simulated Condition	Count	Mean	SD
AUC	Baseline	32	4.08	2.04
	SCI	32	0.07	0.26
	$SCI_{5\text{-}HT}$	32	0.34	0.71
	BWS_{ES}	32	4.53	3.21
	$BWS_{5\text{-}HT}$	32	7.47	2.61
	$BWS_{5\text{-}HT+ES}$	32	6.13	3.82
Fano Factor	Baseline	32	2.13	5.23
	SCI	9	3.29	15.50
	$SCI_{5\text{-}HT}$	26	5.22	11.25
	BWS_{ES}	32	2.05	3.67
	$BWS_{5\text{-}HT}$	32	0.79	2.62
	$BWS_{5\text{-}HT+ES}$	32	1.55	2.92

https://doi.org/10.1371/journal.pcbi.1013866.t007

Table 8. Grand mean and standard deviation (SD) of Fano factor values during active bursting across seeds (n = 32). Relative t-test showed significance between groups.

	Baseline	BWS_{ES}	p-value
Fano factor	0.66 (± 0.06)	1.46 (± 0.22)	< 0.0001

https://doi.org/10.1371/journal.pcbi.1013866.t008

application to proprioceptive afferent axons amplified the effects of reciprocal inhibition, further accentuating excitatory peaks and inhibitory valleys. Simulated BWS locomotion, implemented by adjusting the EMG gain in afferent equations, decreased presynaptic inhibition and consequently restored TA MN firing rates. Combining ES with BWS locomotion produced an activation profile more closely resembling Baseline activity across and within step phases.

Historically, ES has been applied for chronic pain management and spasticity reduction [75,136,137]. The activation pathways of spinal cord stimulation for pain management are understood to be via the large-diameter dorsal column and root fibres that carry propriosensory, mechanosensory, and nociceptive information [138]. GABA INs activate and depress afferent nociceptive signals by antidromic activation of the dorsal column at frequencies, electrode positions, and stimulation amplitudes similar to those of ES for sensorimotor recovery [139,140]. Similarly, ES applied for spasticity reduces the excitatory inputs to MNs through the proprioceptive inhibitory pathways [141,142]. Yet literature in SCI motor recovery places an intense focus on excitation [31,143,144].

Given the heightened inhibitory state of the injured spinal cord, it seems intuitive to return excitation to depressed neurons. However, results from this study suggest that activating the spinal cord with the same proposed mechanisms as pain and spasticity modulation equally activate inhibitory pathways, strengthening an already maladapted inhibition-dominant circuit [86,145]. A more refined and nuanced approach needs to be considered in order to return the required balance of excitation and inhibition to allow phasic activity to propagate. Results in this study suggest that appropriate sensory information must be provided to drive flexor network plastic adaptation towards a less inhibited and more task-specific tuned state. Tonically depressing or exciting, the spinal circuits do not provide the necessary sensory information to provide that plastic tuning [146,147]. This is in agreement with the requirement of propriosensory information for locomotor recovery after SCI [32–34].

The normal sensory processing occurring within the injured spinal cord becomes more stochastic and lacks the necessary bias required to perform the task [133]. As a result, pre-motor polysynaptic connections play a more active role in the expression of muscle tone and activity [148]. By establishing an appropriate balance in excitation and inhibition, repetitive sensory information can reinforce appropriate synaptic adaptations towards a more functional spinal state [70,149]. Results in this study investigate the synaptic mechanisms by which this can be accomplished, and provide a step towards understanding how BWS treadmill training works in concert with neuromodulation therapies [150–152].

The greater deviation in the normalised firing rate indicates increased variability in neuronal population activity after SCI (Fig 4A and 4B). This variability may arise from insufficient excitatory drive to maintain coordinated inhibition and excitation in phase with incoming sensory inputs [133]. Enhancing the excitability of motoneurons and premotor excitatory neurons, while reducing stance-phase inhibition through BWS, can therefore mitigate excessive inhibition of flexor pathways [153–156]. Once the network reaches a sufficiently excitable state that allows the timely propagation of phasic step information, subthreshold electrical stimulation may act as a stabilising mechanism - reinforcing relevant pathways without inducing excessive excitation or inhibition [74,120,121].

Interestingly, firing rate and Fano factor dynamics diverged during burst activity across steps. Although firing rate profiles were similar between steps, the coefficient of variation in spiking activity shifted toward BWS_{ES} values (Fig 8B and Table 8). This divergence may reflect increased neuronal excitation resulting from reduced GABAergic presynaptic inhibition and enhanced facilitation through ES inputs and their downstream synapses. These findings suggest that sensory afferent input combined with BWS and ES produced a broader and more diverse activation of neuronal populations compared with Baseline conditions. The return of stochastic bursting has been linked to improved stepping recovery [133], yet the origins and functional implications of this variability during locomotor rehabilitation after SCI remain poorly understood.

Computational studies such as this are limited in their ability to generalise due to the estimates and tuning that are required to generate the model itself. The simulated flexor reflex loop's SNN architecture is simplistic compared to the complex bidirectional information exchange between the contralateral sides [157,158]. Although the cells were modelled from experimental data, there are errors and missing variables within experiments that have a carry-over effect on computational models. This study utilised LIF and AdEx equations to reduce computational burden and improve simulation runtime. Though previous efforts have incorporated the same approach [69,74], mathematical approximations of firing patterns limit the generalisability [159,160]. However, even with simple estimations, a computational model could provide new hypotheses about the inner workings of neurological systems and unlock novel recovery protocols [140,161].

Future studies could include the experimental verification of these findings via electrophysiological or genetic ablation experiments in rodent models under BWS neuromodulated locomotion contexts. Moreover, extending the model to enable investigation of previous electrophysiological results that uncovered correlations between the appearance of long-latency polysynaptic potentials and recovery of locomotion in spinal rats [35,65,119,121,134,162]. Re-emergence of uninterrupted late-response polysynaptic potentials may be the expression of increased excitability in local spinal networks, re-balancing the inhibitory dominant pre-motor circuity [133,148]. Functional recovery may be mediated by increased magnitude in polysynaptic activity, compensating for the loss in direct excitation [70]. Conversely, this model could be extended to investigate the effects of ES in returning inhibition in a hyperexcitatable environment, such as that of spasticity [23,137]. Currently, there are a diverse number of stimulation paradigms for different causes of spasticity with several hypotheses for the mechanism of action [163]. Such hypotheses cover the inhibition of Ia afferents and stimulation of Aβ fibres to diminish the effect of overactive spinal reflex, reducing muscle tone [164]. Alternative hypotheses suggest the activation of presynaptic inhibition and inhibitory networks within the dorsal column [165]. Finally, extending the computational model to include neuroplastic dynamics could uncover the relationship between neuromodulation and neuroplastic adaptations [118,166,167]. Investigating these effects within an extended computational model would be worthwhile.

Conclusions

The development of a biologically constrained SNN has provided insights into the mechanistic basis of sensory and neuromodulatory integration after SCI. Simulations suggest that BWS locomotion in conjunction with ES returns phasic flexor coordination in an inhibition-dominant environment. In contrast, serotonergic agonists alone increased sensory-driven flexor activation but did not reestablish baseline excitation, while the combination of ES and 5-HT in the absence of

BWS produced network overexcitability. These results highlight that recovering TA MN activity after excessive GABAergic presynaptic inhibition depends on maintaining a dynamic balance between excitation and inhibition within spinal circuits.

Although the current model incorporates key physiological constraints, it remains limited by simplifying assumptions and an incomplete representation of spinal architecture. Future experimental validation will be essential to strengthen the reliability of these inferences. Overall, this work presents a computational framework for probing the combined effects of neuromodulation and sensory afferents on spinal network dynamics, supporting the design of targeted locomotor rehabilitation strategies.

Supporting information

S1 Fig. Visualisation of synapse connection rules.
(TIFF)

S1 Algorithm. Leaky Integrate-and-Fire (LIF) neuron model used to simulate membrane potential dynamics.
(PDF)

S1 Table. TA and GM afferent axon tuning performance measured by Pearson correlation coefficient (CC) and mean absolute error (MAE). All correlations were significant ($p < 0.05$).
(PDF)

S2 Algorithm. Synthesis of Rat EMG From Binary Motor-Unit Action Potential (MUAP)
(PDF)

S2 Fig. Simulated AdEx LIF TA MN single spike. (A) and tonic burst (B) response after receiving a 20 ms and 200 ms stimulation pulse at 670 pA, respectively.
(TIFF)

S2 Table. Bayesian Linear Mixture Model checks for convergence across all conditions.
(PDF)

S3 Table. A hierarchical Linear Mixed Model (LMM) was created for whole step extracted firing rate. Equivalence was established across seeds if $P(|\sigma| < \epsilon) > 0.9$.
(PDF)

S3 Fig. Simulated AdEx LIF V2a IN tonic spiking response after receiving a 200 ms stimulation pulse at 30 pA.
(TIFF)

S4 Fig. Pairwise Pearson correlation results across conditions after mean aggregation across seeds. Steps were concatenated to a single array. All correlations were significant ($p < 0.0001$).
(TIFF)

S4 Table. Results of post-hoc pairwise comparisons between simulated conditions using seed aggregated step firing rate samples in the TA MN during stance and swing phase and their difference.
(PDF)

S5 Fig. Box-and-whisker plots of GABA IN firing rate activity across eight steps for all 32 seeds during Baseline and simulated conditions.
(TIFF)

S5 Table. Descriptive statistics of phase-specific firing rates aggregated over seeds across experimental conditions for V2a and GABA interneurons (INs) following z-score based outlier removal (values exceeding ± 3 standard deviations, were removed). Reported values include the mean, standard deviation (SD), and kurtosis for each locomotor phase (stance and swing) under all experimental conditions.
(PDF)

S6 Fig. Box-and-whisker plots of V2a IN firing rate across eight steps for all 32 seeds during Baseline and simulated conditions.
(TIFF)

Acknowledgments

We would like to thank V. Reggie Edgerton and Parag Gad (University of California, Los Angeles) for the invaluable scientific discussions which led to the conception of the experiment. We would also like to thank Bryce Vissel (St. Vincent's Hospital and University of New South Wales Sydney) for having initiated SCI research at University of Technology Sydney (UTS). Thank you to Howe Zhu (UTS, University of Sydney) for the feedback and support over the years. Finally, thank you to Matthew Gaston of the UTS eResearch team for providing support for and system administration of the Interactive High Performance Computing (iHPC) facility. The computing power and stability of the iHPC system was paramount to running the experiment. This work was supported by the Research Training Program (RTP) scheme from the Department of Education and Training, Australia.

Author contributions

Conceptualization: Raymond Chia.

Data curation: Raymond Chia.

Formal analysis: Raymond Chia.

Funding acquisition: Raymond Chia, Chin-Teng Lin.

Investigation: Raymond Chia.

Methodology: Raymond Chia.

Project administration: Raymond Chia.

Resources: Chin-Teng Lin.

Software: Raymond Chia.

Supervision: Chin-Teng Lin.

Validation: Raymond Chia.

Visualization: Raymond Chia.

Writing – original draft: Raymond Chia.

Writing – review & editing: Raymond Chia, Chin-Teng Lin.

References

1. Dong Y, Peng R, Kang H, Song K, Guo Q, Zhao H, et al. Global incidence, prevalence, and disability of vertebral fractures: a systematic analysis of the global burden of disease study 2019. Spine J. 2022;22(5):857–68. https://doi.org/10.1016/j.spinee.2021.12.007 PMID: 34906740

2. Sezer N, Akkuş S, Uğurlu FG. Chronic complications of spinal cord injury. World J Orthop. 2015;6(1):24–33. https://doi.org/10.5312/wjo.v6.i1.24 PMID: 25621208
3. Nas K, Yazmalar L, ⊠ah V, Aydın A, Öneş K. Rehabilitation of spinal cord injuries. World J Orthop. 2015;6(1):8–16. https://doi.org/10.5312/wjo.v6.i1.8 PMID: 25621206
4. Migliorini C, Tonge B, Taleporos G. Spinal Cord Injury and Mental Health. Aust N Z J Psychiatry. 2008;42(4):309–14. https://doi.org/10.1080/00048670801886080
5. Anderson KD. Targeting recovery: priorities of the spinal cord-injured population. J Neurotrauma. 2004;21(10):1371–83. https://doi.org/10.1089/neu.2004.21.1371 PMID: 15672628
6. Diop M, Epstein D, Gaggero A. Quality of life, health and social costs of patients with spinal cord injury: a systematic review. European Journal of Public Health. 2021;31(Supplement_3). https://doi.org/10.1093/eurpub/ckab165.177
7. Public Health Agency of Canada. 2013. https://www.canada.ca/en/public-health/services/reports-publications/health-promotion-chronic-disease-prevention-canada-research-policy-practice/vol-33-no-3-2013/economic-burden-traumatic-spinal-cord-injury-canada.html
8. McDaid D, Park A-L, Gall A, Purcell M, Bacon M. Understanding and modelling the economic impact of spinal cord injuries in the United Kingdom. Spinal Cord. 2019;57(9):778–88. https://doi.org/10.1038/s41393-019-0285-1 PMID: 31086273
9. DeVivo MJ. Causes and costs of spinal cord injury in the United States. Spinal Cord. 1997;35(12):809–13. https://doi.org/10.1038/sj.sc.3100501 PMID: 9429259
10. Australia A. Spinal Cord Injury in Australia. Sydney, Australia: Accenture. 2020.
11. Hiremath SV, Hogaboom NS, Roscher MR, Worobey LA, Oyster ML, Boninger ML. Longitudinal prediction of quality-of-life scores and locomotion in individuals with traumatic spinal cord injury. Arch Phys Med Rehabil. 2017;98(12):2385–92. https://doi.org/10.1016/j.apmr.2017.05.020 PMID: 28647550
12. Ditunno J, Scivoletto G. Clinical relevance of gait research applied to clinical trials in spinal cord injury. Brain Res Bull. 2009;78(1):35–42. https://doi.org/10.1016/j.brainresbull.2008.09.003 PMID: 18848865
13. Akazawa K, Aldridge JW, Steeves JD, Stein RB. Modulation of stretch reflexes during locomotion in the mesencephalic cat. J Physiol. 1982;329:553–67. https://doi.org/10.1113/jphysiol.1982.sp014319 PMID: 7143259
14. Zhong H, Roy RR, Nakada KK, Zdunowski S, Khalili N, de Leon RD, et al. Accommodation of the spinal cat to a tripping perturbation. Front Physiol. 2012;3:112. https://doi.org/10.3389/fphys.2012.00112 PMID: 22557975
15. Schomburg ED, Petersen N, Barajon I, Hultborn H. Flexor reflex afferents reset the step cycle during fictive locomotion in the cat. Exp Brain Res. 1998;122(3):339–50. https://doi.org/10.1007/s002210050522 PMID: 9808307
16. Little JW, Micklesen P, Umlauf R, Britell C. Lower extremity manifestations of spasticity in chronic spinal cord injury. Am J Phys Med Rehabil. 1989;68(1):32–6. https://doi.org/10.1097/00002060-198902000-00009 PMID: 2917056
17. Schmit BD, McKenna-Cole A, Rymer WZ. Flexor reflexes in chronic spinal cord injury triggered by imposed ankle rotation. Muscle Nerve. 2000;23(5):793–803. https://doi.org/10.1002/(sici)1097-4598(200005)23:5<793::aid-mus18>3.0.co;2-t PMID: 10797404
18. Harnie J, Doelman A, de Vette E, Audet J, Desrochers E, Gaudreault N, et al. The recovery of standing and locomotion after spinal cord injury does not require task-specific training. Elife. 2019;8:e50134. https://doi.org/10.7554/eLife.50134 PMID: 31825306
19. Beauparlant J, van den Brand R, Barraud Q, Friedli L, Musienko P, Dietz V, et al. Undirected compensatory plasticity contributes to neuronal dysfunction after severe spinal cord injury. Brain. 2013;136(Pt 11):3347–61. https://doi.org/10.1093/brain/awt204 PMID: 24080153
20. Lynskey JV, Belanger A, Jung R. Activity-dependent plasticity in spinal cord injury. J Rehabil Res Dev. 2008;45(2):229–40. https://doi.org/10.1682/jrrd.2007.03.0047 PMID: 18566941
21. Edgerton VR, Tillakaratne NJK, Bigbee AJ, de Leon RD, Roy RR. Plasticity of the spinal neural circuitry after injury. Annu Rev Neurosci. 2004;27:145–67. https://doi.org/10.1146/annurev.neuro.27.070203.144308 PMID: 15217329
22. Bellardita C, Caggiano V, Leiras R, Caldeira V, Fuchs A, Bouvier J, et al. Spatiotemporal correlation of spinal network dynamics underlying spasms in chronic spinalized mice. Elife. 2017;6:e23011. https://doi.org/10.7554/eLife.23011 PMID: 28191872
23. Dimitrijevic MM, Dimitrijevic MR, Illis LS, Nakajima K, Sharkey PC, Sherwood AM. Spinal cord stimulation for the control of spasticity in patients with chronic spinal cord injury: I. Clinical observations. Cent Nerv Syst Trauma. 1986;3(2):129–44. https://doi.org/10.1089/cns.1986.3.129 PMID: 3490312
24. Pinter MM, Gerstenbrand F, Dimitrijevic MR. Epidural electrical stimulation of posterior structures of the human lumbosacral cord: 3. Control Of spasticity. Spinal Cord. 2000;38(9):524–31. https://doi.org/10.1038/sj.sc.3101040 PMID: 11035472
25. Cowley KC, Schmidt BJ. Effects of inhibitory amino acid antagonists on reciprocal inhibitory interactions during rhythmic motor activity in the in vitro neonatal rat spinal cord. J Neurophysiol. 1995;74(3):1109–17. https://doi.org/10.1152/jn.1995.74.3.1109 PMID: 7500136
26. McKay WB, Ovechkin AV, Vitaz TW, Terson de Paleville DGL, Harkema SJ. Long-lasting involuntary motor activity after spinal cord injury. Spinal Cord. 2011;49(1):87–93. https://doi.org/10.1038/sc.2010.73 PMID: 20585326
27. Harkema S, Gerasimenko Y, Hodes J, Burdick J, Angeli C, Chen Y, et al. Effect of epidural stimulation of the lumbosacral spinal cord on voluntary movement, standing, and assisted stepping after motor complete paraplegia: a case study. Lancet. 2011;377(9781):1938–47. https://doi.org/10.1016/S0140-6736(11)60547-3 PMID: 21601270

28. Gad P, Gerasimenko Y, Zdunowski S, Turner A, Sayenko D, Lu DC, et al. Weight bearing over-ground stepping in an exoskeleton with non-invasive spinal cord neuromodulation after motor complete Paraplegia. Front Neurosci. 2017;11:333. https://doi.org/10.3389/fnins.2017.00333 PMID: 28642680
29. Rejc E, Angeli CA, Atkinson D, Harkema SJ. Motor recovery after activity-based training with spinal cord epidural stimulation in a chronic motor complete paraplegic. Sci Rep. 2017;7(1):13476. https://doi.org/10.1038/s41598-017-14003-w PMID: 29074997
30. Rowald A, Komi S, Demesmaeker R, Baaklini E, Hernandez-Charpak SD, Paoles E, et al. Activity-dependent spinal cord neuromodulation rapidly restores trunk and leg motor functions after complete paralysis. Nat Med. 2022;28(2):260–71. https://doi.org/10.1038/s41591-021-01663-5 PMID: 35132264
31. Lorach H, Galvez A, Spagnolo V, Martel F, Karakas S, Intering N, et al. Walking naturally after spinal cord injury using a brain-spine interface. Nature. 2023;618(7963):126–33. https://doi.org/10.1038/s41586-023-06094-5 PMID: 37225984
32. Takeoka A, Vollenweider I, Courtine G, Arber S. Muscle spindle feedback directs locomotor recovery and circuit reorganization after spinal cord injury. Cell. 2014;159(7):1626–39. https://doi.org/10.1016/j.cell.2014.11.019 PMID: 25525880
33. Takeoka A, Arber S. Functional local proprioceptive feedback circuits initiate and maintain locomotor recovery after spinal cord injury. Cell Rep. 2019;27(1):71-85.e3. https://doi.org/10.1016/j.celrep.2019.03.010 PMID: 30943416
34. Akay T, Tourtellotte WG, Arber S, Jessell TM. Degradation of mouse locomotor pattern in the absence of proprioceptive sensory feedback. Proc Natl Acad Sci U S A. 2014;111(47):16877–82. https://doi.org/10.1073/pnas.1419045111 PMID: 25389309
35. Lavrov I, Gerasimenko YP, Ichiyama RM, Courtine G, Zhong H, Roy RR, et al. Plasticity of spinal cord reflexes after a complete transection in adult rats: relationship to stepping ability. Journal of Neurophysiology. 2006;96(4):1699–710. https://doi.org/10.1152/jn.00325.2006
36. Flynn JR, Graham BA, Galea MP, Callister RJ. The role of propriospinal interneurons in recovery from spinal cord injury. Neuropharmacology. 2011;60(5):809–22. https://doi.org/10.1016/j.neuropharm.2011.01.016
37. Côté M-P, Murray LM, Knikou M. Spinal control of locomotion: individual neurons, their circuits and functions. Front Physiol. 2018;9:784. https://doi.org/10.3389/fphys.2018.00784 PMID: 29988534
38. Tillakaratne NJK, Duru P, Fujino H, Zhong H, Xiao MS, Edgerton VR, et al. Identification of interneurons activated at different inclines during treadmill locomotion in adult rats. J Neurosci Res. 2014;92(12):1714–22. https://doi.org/10.1002/jnr.23437 PMID: 24975393
39. Liu P, Zhang X, He X, Jiang Z, Wang Q, Lu Y. Spinal GABAergic neurons are under feed-forward inhibitory control driven by Aδ and C fibers in Gad2 td-Tomato mice. Mol Pain. 2021;17:1744806921992620. https://doi.org/10.1177/1744806921992620 PMID: 33586515
40. Nakamura Y, Kurabe M, Matsumoto M, Sato T, Miyashita S, Hoshina K, et al. Cerebrospinal fluid-contacting neuron tracing reveals structural and functional connectivity for locomotion in the mouse spinal cord. Elife. 2023;12:e83108. https://doi.org/10.7554/eLife.83108 PMID: 36805807
41. Zagoraiou L, Akay T, Martin JF, Brownstone RM, Jessell TM, Miles GB. A cluster of cholinergic premotor interneurons modulates mouse locomotor activity. Neuron. 2009;64(5):645–62. https://doi.org/10.1016/j.neuron.2009.10.017 PMID: 20005822
42. Lu DC, Niu T, Alaynick WA. Molecular and cellular development of spinal cord locomotor circuitry. Front Mol Neurosci. 2015;8:25. https://doi.org/10.3389/fnmol.2015.00025 PMID: 26136656
43. Nascimento F, Broadhead MJ, Tetringa E, Tsape E, Zagoraiou L, Miles GB. Synaptic mechanisms underlying modulation of locomotor-related motoneuron output by premotor cholinergic interneurons. Elife. 2020;9:e54170. https://doi.org/10.7554/eLife.54170 PMID: 32081133
44. Niu J, Ding L, Li JJ, Kim H, Liu J, Li H, et al. Modality-based organization of ascending somatosensory axons in the direct dorsal column pathway. J Neurosci. 2013;33(45):17691–709. https://doi.org/10.1523/JNEUROSCI.3429-13.2013 PMID: 24198362
45. Brownstone RM, Bui TV, Stifani N. Spinal circuits for motor learning. Curr Opin Neurobiol. 2015;33:166–73. https://doi.org/10.1016/j.conb.2015.04.007 PMID: 25978563
46. Laliberte AM, Goltash S, Lalonde NR, Bui TV. Propriospinal neurons: essential elements of locomotor control in the intact and possibly the injured spinal cord. Front Cell Neurosci. 2019;13:512. https://doi.org/10.3389/fncel.2019.00512 PMID: 31798419
47. Flynn JR, Conn VL, Boyle KA, Hughes DI, Watanabe M, Velasquez T, et al. Anatomical and molecular properties of long descending propriospinal neurons in mice. Front Neuroanat. 2017;11. https://doi.org/10.3389/fnana.2017.00005
48. Eisdorfer JT, Smit RD, Keefe KM, Lemay MA, Smith GM, Spence AJ. Epidural electrical stimulation: a review of plasticity mechanisms that are hypothesized to underlie enhanced recovery from spinal cord injury with stimulation. Front Mol Neurosci. 2020;13:163. https://doi.org/10.3389/fnmol.2020.00163 PMID: 33013317
49. Filli L, Engmann AK, Zörner B, Weinmann O, Moraitis T, Gullo M, et al. Bridging the gap: a reticulo-propriospinal detour bypassing an incomplete spinal cord injury. J Neurosci. 2014;34(40):13399–410. https://doi.org/10.1523/JNEUROSCI.0701-14.2014 PMID: 25274818
50. Taccola G, Sayenko D, Gad P, Gerasimenko Y, Edgerton VR. And yet it moves: recovery of volitional control after spinal cord injury. Prog Neurobiol. 2018;160:64–81. https://doi.org/10.1016/j.pneurobio.2017.10.004 PMID: 29102670
51. Gerasimenko Y, Musienko P, Bogacheva I, Moshonkina T, Savochin A, Lavrov I, et al. Propriospinal bypass of the serotonergic system that can facilitate stepping. J Neurosci. 2009;29(17):5681–9. https://doi.org/10.1523/JNEUROSCI.6058-08.2009 PMID: 19403834
52. Crone SA, Quinlan KA, Zagoraiou L, Droho S, Restrepo CE, Lundfald L, et al. Genetic ablation of V2a ipsilateral interneurons disrupts left-right locomotor coordination in mammalian spinal cord. Neuron. 2008;60(1):70–83. https://doi.org/10.1016/j.neuron.2008.08.009 PMID: 18940589
53. Zhong G, Droho S, Crone SA, Dietz S, Kwan AC, Webb WW, et al. Electrophysiological characterization of V2a interneurons and their locomotor-related activity in the neonatal mouse spinal cord. J Neurosci. 2010;30(1):170–82. https://doi.org/10.1523/JNEUROSCI.4849-09.2010 PMID: 20053899

54. Crone SA, Zhong G, Harris-Warrick R, Sharma K. In mice lacking V2a interneurons, gait depends on speed of locomotion. J Neurosci. 2009;29(21):7098–109. https://doi.org/10.1523/JNEUROSCI.1206-09.2009 PMID: 19474336

55. Dougherty KJ, Kiehn O. Firing and cellular properties of V2a interneurons in the rodent spinal cord. J Neurosci. 2010;30(1):24–37. https://doi.org/10.1523/JNEUROSCI.4821-09.2010 PMID: 20053884

56. Bourane S, Grossmann KS, Britz O, Dalet A, Del Barrio MG, Stam FJ, et al. Identification of a spinal circuit for light touch and fine motor control. Cell. 2015;160(3):503–15. https://doi.org/10.1016/j.cell.2015.01.011 PMID: 25635458

57. Al-Mosawie A, Wilson JM, Brownstone RM. Heterogeneity of V2-derived interneurons in the adult mouse spinal cord. Eur J Neurosci. 2007;26(11):3003–15. https://doi.org/10.1111/j.1460-9568.2007.05907.x PMID: 18028108

58. Li W-Y, Deng L-X, Zhai F-G, Wang X-Y, Li Z-G, Wang Y. Chx10+V2a interneurons in spinal motor regulation and spinal cord injury. Neural Regen Res. 2023;18(5):933–9. https://doi.org/10.4103/1673-5374.355746 PMID: 36254971

59. Hayashi M, Hinckley CA, Driscoll SP, Moore NJ, Levine AJ, Hilde KL, et al. Graded arrays of spinal and supraspinal V2a interneuron subtypes underlie forelimb and hindlimb motor control. Neuron. 2018;97(4):869-884.e5. https://doi.org/10.1016/j.neuron.2018.01.023 PMID: 29398364

60. Song J, Dahlberg E, El Manira A. V2a interneuron diversity tailors spinal circuit organization to control the vigor of locomotor movements. Nat Commun. 2018;9(1):3370. https://doi.org/10.1038/s41467-018-05827-9 PMID: 30135498

61. Kathe C, Skinnider MA, Hutson TH, Regazzi N, Gautier M, Demesmaeker R, et al. The neurons that restore walking after paralysis. Nature. 2022;611(7936):540–7. https://doi.org/10.1038/s41586-022-05385-7 PMID: 36352232

62. Courtine G, Song B, Roy RR, Zhong H, Herrmann JE, Ao Y, et al. Recovery of supraspinal control of stepping via indirect propriospinal relay connections after spinal cord injury. Nat Med. 2008;14(1):69–74. https://doi.org/10.1038/nm1682 PMID: 18157143

63. Truchon C, Fallah N, Santos A, Vachon J, Noonan VK, Cheng CL. Impact of therapy on recovery during rehabilitation in patients with traumatic spinal cord injury. J Neurotrauma. 2017;34(20):2901–9. https://doi.org/10.1089/neu.2016.4932 PMID: 28493787

64. Capogrosso M, Milekovic T, Borton D, Wagner F, Moraud EM, Mignardot J-B, et al. A brain-spine interface alleviating gait deficits after spinal cord injury in primates. Nature. 2016;539(7628):284–8. https://doi.org/10.1038/nature20118 PMID: 27830790

65. Gad P, Lavrov I, Shah P, Zhong H, Roy RR, Edgerton VR, et al. Neuromodulation of motor-evoked potentials during stepping in spinal rats. J Neurophysiol. 2013;110(6):1311–22. https://doi.org/10.1152/jn.00169.2013 PMID: 23761695

66. Courtine G, Gerasimenko Y, van den Brand R, Yew A, Musienko P, Zhong H, et al. Transformation of nonfunctional spinal circuits into functional states after the loss of brain input. Nat Neurosci. 2009;12(10):1333–42. https://doi.org/10.1038/nn.2401 PMID: 19767747

67. Gad P, Choe J, Shah P, Garcia-Alias G, Rath M, Gerasimenko Y, et al. Sub-threshold spinal cord stimulation facilitates spontaneous motor activity in spinal rats. J Neuroeng Rehabil. 2013;10:108. https://doi.org/10.1186/1743-0003-10-108 PMID: 24156340

68. Gerasimenko Y, Gorodnichev R, Puhov A, Moshonkina T, Savochin A, Selionov V, et al. Initiation and modulation of locomotor circuitry output with multisite transcutaneous electrical stimulation of the spinal cord in noninjured humans. J Neurophysiol. 2015;113(3):834–42. https://doi.org/10.1152/jn.00609.2014 PMID: 25376784

69. Moraud EM, Capogrosso M, Formento E, Wenger N, DiGiovanna J, Courtine G, et al. Mechanisms underlying the neuromodulation of spinal circuits for correcting gait and balance deficits after spinal cord injury. Neuron. 2016;89(4):814–28. https://doi.org/10.1016/j.neuron.2016.01.009 PMID: 26853304

70. Edgerton VR, Courtine G, Gerasimenko YP, Lavrov I, Ichiyama RM, Fong AJ, et al. Training locomotor networks. Brain Res Rev. 2008;57(1):241–54. https://doi.org/10.1016/j.brainresrev.2007.09.002 PMID: 18022244

71. Capogrosso M, Wenger N, Raspopovic S, Musienko P, Beauparlant J, Bassi Luciani L, et al. A computational model for epidural electrical stimulation of spinal sensorimotor circuits. J Neurosci. 2013;33(49):19326–40. https://doi.org/10.1523/JNEUROSCI.1688-13.2013 PMID: 24305828

72. Angeli CA, Edgerton VR, Gerasimenko YP, Harkema SJ. Altering spinal cord excitability enables voluntary movements after chronic complete paralysis in humans. Brain. 2014;137(Pt 5):1394–409. https://doi.org/10.1093/brain/awu038 PMID: 24713270

73. Danner SM, Hofstoetter US, Freundl B, Binder H, Mayr W, Rattay F, et al. Human spinal locomotor control is based on flexibly organized burst generators. Brain. 2015;138(Pt 3):577–88. https://doi.org/10.1093/brain/awu372 PMID: 25582580

74. Formento E, Minassian K, Wagner F, Mignardot JB, Le Goff-Mignardot CG, Rowald A, et al. Electrical spinal cord stimulation must preserve proprioception to enable locomotion in humans with spinal cord injury. Nat Neurosci. 2018;21(12):1728–41. https://doi.org/10.1038/s41593-018-0262-6 PMID: 30382196

75. Caylor J, Reddy R, Yin S, Cui C, Huang M, Huang C, et al. Spinal cord stimulation in chronic pain: evidence and theory for mechanisms of action. Bioelectron Med. 2019;5:12. https://doi.org/10.1186/s42234-019-0023-1 PMID: 31435499

76. Danner SM, Shevtsova NA, Frigon A, Rybak IA. Computational modeling of spinal circuits controlling limb coordination and gaits in quadrupeds. Elife. 2017;6:e31050. https://doi.org/10.7554/eLife.31050 PMID: 29165245

77. Zhang H, Shevtsova NA, Deska-Gauthier D, Mackay C, Dougherty KJ, Danner SM, et al. The role of V3 neurons in speed-dependent interlimb coordination during locomotion in mice. Elife. 2022;11:e73424. https://doi.org/10.7554/eLife.73424 PMID: 35476640

78. Rybak IA, Shevtsova NA, Lafreniere-Roula M, McCrea DA. Modelling spinal circuitry involved in locomotor pattern generation: insights from deletions during fictive locomotion. J Physiol. 2006;577(Pt 2):617–39. https://doi.org/10.1113/jphysiol.2006.118703 PMID: 17008376

79. Rybak IA, Stecina K, Shevtsova NA, McCrea DA. Modelling spinal circuitry involved in locomotor pattern generation: insights from the effects of afferent stimulation. The Journal of Physiology. 2006;577(2):641–58. https://doi.org/10.1113/jphysiol.2006.118711

80. Shik ML, Severin FV, Orlovsky GN. Control of walking and running by means of electrical stimulation of the mesencephalon. Electroencephalogr Clin Neurophysiol. 1969;26(5):549. PMID: 4181500

81. Grillner S. Neurobiological bases of rhythmic motor acts in vertebrates. Science. 1985;228(4696):143–9. https://doi.org/10.1126/science.3975635 PMID: 3975635

82. Danner SM, Wilshin SD, Shevtsova NA, Rybak IA. Central control of interlimb coordination and speed-dependent gait expression in quadrupeds. J Physiol. 2016;594(23):6947–67. https://doi.org/10.1113/JP272787 PMID: 27633893

83. Di Russo A, Stanev D, Sabnis A, Danner SM, Ausborn J, Armand S, et al. Investigating the roles of reflexes and central pattern generators in the control and modulation of human locomotion using a physiologically plausible neuromechanical model. J Neural Eng. 2023;20(6):10.1088/1741-2552/acfdcc. https://doi.org/10.1088/1741-2552/acfdcc PMID: 37757805

84. Stimberg M, Brette R, Goodman DF. Brian 2, an intuitive and efficient neural simulator. Elife. 2019;8:e47314. https://doi.org/10.7554/eLife.47314 PMID: 31429824

85. Leblond H, L'Esperance M, Orsal D, Rossignol S. Treadmill locomotion in the intact and spinal mouse. J Neurosci. 2003;23(36):11411–9. https://doi.org/10.1523/JNEUROSCI.23-36-11411.2003 PMID: 14673005

86. Khristy W, Ali NJ, Bravo AB, de Leon R, Roy RR, Zhong H, et al. Changes in GABA(A) receptor subunit gamma 2 in extensor and flexor motoneurons and astrocytes after spinal cord transection and motor training. Brain Res. 2009;1273:9–17. https://doi.org/10.1016/j.brainres.2009.03.060 PMID: 19358834

87. Kristiansen M, Odderskær N, Kristensen DH. Effect of body weight support on muscle activation during walking on a lower body positive pressure treadmill. J Electromyogr Kinesiol. 2019;48:9–16. https://doi.org/10.1016/j.jelekin.2019.05.021 PMID: 31176846

88. Bui TV, Cushing S, Dewey D, Fyffe RE, Rose PK. Comparison of the morphological and electrotonic properties of Renshaw cells, Ia inhibitory interneurons, and motoneurons in the cat. J Neurophysiol. 2003;90(5):2900–18. https://doi.org/10.1152/jn.00533.2003 PMID: 12878716

89. Jankowska E, Roberts WJ. Synaptic actions of single interneurones mediating reciprocal Ia inhibition of motoneurones. The Journal of Physiology. 1972;222(3):623–42. https://doi.org/10.1113/jphysiol.1972.sp009818

90. Edgley SA, Jankowska E. An interneuronal relay for group I and II muscle afferents in the midlumbar segments of the cat spinal cord.. The Journal of Physiology. 1987;389(1):647–74. https://doi.org/10.1113/jphysiol.1987.sp016676

91. Rudomin P. Presynaptic inhibition of muscle spindle and tendon organ afferents in the mammalian spinal cord. Trends Neurosci. 1990;13(12):499–505. https://doi.org/10.1016/0166-2236(90)90084-n PMID: 1703681

92. Jankowska E. Interneuronal relay in spinal pathways from proprioceptors. Prog Neurobiol. 1992;38(4):335–78. https://doi.org/10.1016/0301-0082(92)90024-9 PMID: 1315446

93. Rudomin P, Schmidt RF. Presynaptic inhibition in the vertebrate spinal cord revisited. Exp Brain Res. 1999;129(1):1–37. https://doi.org/10.1007/s002210050933 PMID: 10550500

94. Jankowska E. Spinal interneurons. Neuroscience in the 21st Century: From Basic to Clinical. New York: Springer; 2013. p. 1063–99.

95. Dougherty KJ, Zagoraiou L, Satoh D, Rozani I, Doobar S, Arber S, et al. Locomotor rhythm generation linked to the output of spinal shox2 excitatory interneurons. Neuron. 2013;80(4):920–33. https://doi.org/10.1016/j.neuron.2013.08.015 PMID: 24267650

96. Talpalar AE, Endo T, Löw P, Borgius L, Hägglund M, Dougherty KJ, et al. Identification of minimal neuronal networks involved in flexor-extensor alternation in the mammalian spinal cord. Neuron. 2011;71(6):1071–84. https://doi.org/10.1016/j.neuron.2011.07.011 PMID: 21943604

97. Fink AJP, Croce KR, Huang ZJ, Abbott LF, Jessell TM, Azim E. Presynaptic inhibition of spinal sensory feedback ensures smooth movement. Nature. 2014;509(7498):43–8. https://doi.org/10.1038/nature13276 PMID: 24784215

98. Bui TV, Stifani N, Akay T, Brownstone RM. Spinal microcircuits comprising dI3 interneurons are necessary for motor functional recovery following spinal cord transection. Elife. 2016;5:e21715. https://doi.org/10.7554/eLife.21715 PMID: 27977000

99. Koch SC, Del Barrio MG, Dalet A, Gatto G, Günther T, Zhang J, et al. RORβ spinal interneurons gate sensory transmission during locomotion to secure a fluid walking gait. Neuron. 2017;96(6):1419-1431.e5. https://doi.org/10.1016/j.neuron.2017.11.011 PMID: 29224725

100. Macdonald DB. Intraoperative motor evoked potential monitoring: overview and update. J Clin Monit Comput. 2006;20(5):347–77. https://doi.org/10.1007/s10877-006-9033-0 PMID: 16832580

101. Naud R, Marcille N, Clopath C, Gerstner W. Firing patterns in the adaptive exponential integrate-and-fire model. Biol Cybern. 2008;99(4–5):335–47. https://doi.org/10.1007/s00422-008-0264-7 PMID: 19011922

102. Husch A, Dietz SB, Hong DN, Harris-Warrick RM. Adult spinal V2a interneurons show increased excitability and serotonin-dependent bistability. J Neurophysiol. 2015;113(4):1124–34. https://doi.org/10.1152/jn.00741.2014 PMID: 25520435

103. Gorassini M, Eken T, Bennett DJ, Kiehn O, Hultborn H. Activity of hindlimb motor units during locomotion in the conscious rat. J Neurophysiol. 2000;83(4):2002–11. https://doi.org/10.1152/jn.2000.83.4.2002 PMID: 10758110

104. Prochazka A. Quantifying proprioception. Prog Brain Res. 1999;123:133–42. https://doi.org/10.1016/s0079-6123(08)62850-2 PMID: 10635710

105. Lüscher C, Streit J, Lipp P, Lüscher HR. Action potential propagation through embryonic dorsal root ganglion cells in culture. II. Decrease of conduction reliability during repetitive stimulation. J Neurophysiol. 1994;72(2):634–43. https://doi.org/10.1152/jn.1994.72.2.634 PMID: 7983525

106. Bostock H, Sears TA. The internodal axon membrane: electrical excitability and continuous conduction in segmental demyelination. J Physiol. 1978;280:273–301. https://doi.org/10.1113/jphysiol.1978.sp012384 PMID: 690876

107. Cowley KC, Zaporozhets E, Schmidt BJ. Propriospinal transmission of the locomotor command signal in the neonatal rat. Ann N Y Acad Sci. 2010;1198:42–53. https://doi.org/10.1111/j.1749-6632.2009.05421.x PMID: 20536919

108. Baek M, Pivetta C, Liu J-P, Arber S, Dasen JS. Columnar-intrinsic cues shape premotor input specificity in locomotor circuits. Cell Rep. 2017;21(4):867–77. https://doi.org/10.1016/j.celrep.2017.10.004 PMID: 29069594

109. Khalki L, Sadlaoud K, Lerond J, Coq J-O, Brezun J-M, Vinay L, et al. Changes in innervation of lumbar motoneurons and organization of premotor network following training of transected adult rats. Exp Neurol. 2018;299(Pt A):1–14. https://doi.org/10.1016/j.expneurol.2017.09.002 PMID: 28917641

110. Bui TV, Akay T, Loubani O, Hnasko TS, Jessell TM, Brownstone RM. Circuits for grasping: spinal dI3 interneurons mediate cutaneous control of motor behavior. Neuron. 2013;78(1):191–204. https://doi.org/10.1016/j.neuron.2013.02.007 PMID: 23583114

111. Caillet AH, Phillips ATM, Farina D, Modenese L. Mathematical relationships between spinal motoneuron properties. Elife. 2022;11:e76489. https://doi.org/10.7554/eLife.76489 PMID: 35848819

112. Özyurt MG, Ojeda-Alonso J, Beato M, Nascimento F. In vitro longitudinal lumbar spinal cord preparations to study sensory and recurrent motor microcircuits of juvenile mice. J Neurophysiol. 2022;128(3):711–26. https://doi.org/10.1152/jn.00184.2022 PMID: 35946796

113. Booth V, Rinzel J, Kiehn O. Compartmental model of vertebrate motoneurons for Ca2+-dependent spiking and plateau potentials under pharmacological treatment. Journal of Neurophysiology. 1997;78(6):3371–85. https://doi.org/10.1152/jn.1997.78.6.3371

114. Munson JB, Fleshman JW, Sypert GW. Properties of single-fiber spindle group II EPSPs in triceps surae motoneurons. J Neurophysiol. 1980;44(4):713–25. https://doi.org/10.1152/jn.1980.44.4.713 PMID: 6448918

115. Segev I, Fleshman JW Jr, Burke RE. Computer simulation of group Ia EPSPs using morphologically realistic models of cat alpha-motoneurons. J Neurophysiol. 1990;64(2):648–60. https://doi.org/10.1152/jn.1990.64.2.648 PMID: 2213137

116. Hochman S, Shreckengost J, Kimura H, Quevedo J. Presynaptic inhibition of primary afferents by depolarization: observations supporting nontraditional mechanisms. Ann N Y Acad Sci. 2010;1198:140–52. https://doi.org/10.1111/j.1749-6632.2010.05436.x PMID: 20536928

117. Lalonde NR, Bui TV. Do spinal circuits still require gating of sensory information by presynaptic inhibition after spinal cord injury?. Current Opinion in Physiology. 2021;19:113–8. https://doi.org/10.1016/j.cophys.2020.10.001

118. Naumann LB, Sprekeler H. Presynaptic inhibition rapidly stabilises recurrent excitation in the face of plasticity. PLoS Comput Biol. 2020;16(8):e1008118. https://doi.org/10.1371/journal.pcbi.1008118 PMID: 32764742

119. Lavrov I, Courtine G, Dy CJ, van den Brand R, Fong AJ, Gerasimenko Y, et al. Facilitation of stepping with epidural stimulation in spinal rats: role of sensory input. J Neurosci. 2008;28(31):7774–80. https://doi.org/10.1523/JNEUROSCI.1069-08.2008 PMID: 18667609

120. Ichiyama RM, Gerasimenko Y, Jindrich DL, Zhong H, Roy RR, Edgerton VR. Dose dependence of the 5-HT agonist quipazine in facilitating spinal stepping in the rat with epidural stimulation. Neurosci Lett. 2008;438(3):281–5. https://doi.org/10.1016/j.neulet.2008.04.080 PMID: 18490105

121. Gerasimenko YP, Ichiyama RM, Lavrov IA, Courtine G, Cai L, Zhong H, et al. Epidural spinal cord stimulation plus quipazine administration enable stepping in complete spinal adult rats. J Neurophysiol. 2007;98(5):2525–36. https://doi.org/10.1152/jn.00836.2007 PMID: 17855582

122. Softky WR, Koch C. The highly irregular firing of cortical cells is inconsistent with temporal integration of random EPSPs. J Neurosci. 1993;13(1):334–50. https://doi.org/10.1523/JNEUROSCI.13-01-00334.1993 PMID: 8423479

123. Wang K, Wei A, Fu Y, Wang T, Gao X, Fu B, et al. State-dependent modulation of thalamocortical oscillations by gamma light flicker with different frequencies, intensities, and duty cycles. Front Neuroinform. 2022;16:968907. https://doi.org/10.3389/fninf.2022.968907 PMID: 36081653

124. Gill JV, Lerman GM, Chong E, Rinberg D, Shoham S. Illuminating neural computation using precision optogenetics-controlled synthetic perception. In: Papagiakoumou E, editor. All-optical methods to study neuronal function. New York: Humana. 2023. p. 363–92. https://doi.org/10.1007/978-1-0716-2764-8_12

125. Triplett MA, Gajowa M, Antin B, Sadahiro M, Adesnik H, Paninski L. Rapid learning of neural circuitry from holographic ensemble stimulation enabled by model-based compressed sensing. Nat Neurosci. 2025;28(10):2154–65. https://doi.org/10.1038/s41593-025-02053-7 PMID: 40962967

126. Sourmpis C, Petersen CC, Gerstner W, Bellec G. Biologically informed cortical models predict optogenetic perturbations. eLife Sciences Publications, Ltd.; 2025. https://doi.org/10.7554/elife.106827.1

127. Day SJ, Hulliger M. Experimental simulation of cat electromyogram: evidence for algebraic summation of motor-unit action-potential trains. J Neurophysiol. 2001;86(5):2144–58. https://doi.org/10.1152/jn.2001.86.5.2144 PMID: 11698507

128. Homan MD, Gelman A. The No-U-Turn sampler: adaptively setting path lengths in Hamiltonian Monte Carlo. J Mach Learn Res. 2014;15(1):1593–623.

129. Salvatier J, Wiecki TV, Fonnesbeck C. Probabilistic programming in Python using PyMC3. PeerJ Computer Science. 2016;2:e55. https://doi.org/10.7717/peerj-cs.55

130. Gelman A, Rubin DB. Inference from Iterative Simulation Using Multiple Sequences. Statist Sci. 1992;7(4). https://doi.org/10.1214/ss/1177011136

131. Ritter LK, Tresch MC, Heckman CJ, Manuel M, Tysseling VM. Characterization of motor units in behaving adult mice shows a wide primary range. J Neurophysiol. 2014;112(3):543–51. https://doi.org/10.1152/jn.00108.2014 PMID: 24805075

132. Tresch MC, Kiehn O. Synchronization of motor neurons during locomotion in the neonatal rat: predictors and mechanisms. J Neurosci. 2002;22(22):9997–10008. https://doi.org/10.1523/JNEUROSCI.22-22-09997.2002 PMID: 12427857

133. Gad P, Roy RR, Choe J, Creagmile J, Zhong H, Gerasimenko Y, et al. Electrophysiological biomarkers of neuromodulatory strategies to recover motor function after spinal cord injury. J Neurophysiol. 2015;113(9):3386–96. https://doi.org/10.1152/jn.00918.2014 PMID: 25695648

134. Gerasimenko YP, Lavrov IA, Courtine G, Ichiyama RM, Dy CJ, Zhong H, et al. Spinal cord reflexes induced by epidural spinal cord stimulation in normal awake rats. J Neurosci Methods. 2006;157(2):253–63. https://doi.org/10.1016/j.jneumeth.2006.05.004 PMID: 16764937

135. Roy RR, Hutchison DL, Pierotti DJ, Hodgson JA, Edgerton VR. EMG patterns of rat ankle extensors and flexors during treadmill locomotion and swimming. J Appl Physiol (1985). 1991;70(6):2522–9. https://doi.org/10.1152/jappl.1991.70.6.2522 PMID: 1885445

136. Stewart JE, Barbeau H, Gauthier S. Modulation of locomotor patterns and spasticity with clonidine in spinal cord injured patients. Can J Neurol Sci. 1991;18(3):321–32. https://doi.org/10.1017/s0317167100031887 PMID: 1913367

137. Edgerton VR, Roy RR. Spasticity: a switch from inhibition to excitation. Nat Med. 2010;16(3):270–1. https://doi.org/10.1038/nm0310-270 PMID: 20208512

138. Guan Y, Bradley K, Parker JL, Krames ES, Linderoth B. Spinal cord stimulation: mechanisms of action. In: Krames ES, Peckham PH, Rezai AR, editors. Neuromodulation. 2nd ed. Academic Press; 2018. p. 161–78.

139. Meuwissen KPV, de Vries LE, Gu JW, Zhang TC, Joosten EAJ. Burst and tonic spinal cord stimulation both activate spinal GABAergic mechanisms to attenuate pain in a rat model of chronic neuropathic pain. Pain Pract. 2020;20(1):75–87. https://doi.org/10.1111/papr.12831 PMID: 31424152

140. Wenger N, Moraud EM, Gandar J, Musienko P, Capogrosso M, Baud L, et al. Spatiotemporal neuromodulation therapies engaging muscle synergies improve motor control after spinal cord injury. Nat Med. 2016;22(2):138–45. https://doi.org/10.1038/nm.4025 PMID: 26779815

141. Alashram AR, Padua E, Raju M, Romagnoli C, Annino G. Transcutaneous spinal cord stimulation effects on spasticity in patients with spinal cord injury: a systematic review. J Spinal Cord Med. 2023;46(4):582–9. https://doi.org/10.1080/10790268.2021.2000200 PMID: 34855565

142. Mahrous A, Birch D, Heckman CJ, Tysseling V. Muscle spasms after spinal cord injury stem from changes in motoneuron excitability and synaptic inhibition, not synaptic excitation. J Neurosci. 2024;44(1):e1695232023. https://doi.org/10.1523/JNEUROSCI.1695-23.2023 PMID: 37949656

143. Alluin O, Delivet-Mongrain H, Rossignol S. Inducing hindlimb locomotor recovery in adult rat after complete thoracic spinal cord section using repeated treadmill training with perineal stimulation only. J Neurophysiol. 2015;114(3):1931–46. https://doi.org/10.1152/jn.00416.2015 PMID: 26203108

144. Minassian K, Hofstoetter US. Spinal cord stimulation and augmentative control strategies for leg movement after spinal paralysis in humans. CNS Neurosci Ther. 2016;22(4):262–70. https://doi.org/10.1111/cns.12530 PMID: 26890324

145. Edgerton VR, Leon RD, Harkema SJ, Hodgson JA, London N, Reinkensmeyer DJ, et al. Retraining the injured spinal cord. J Physiol. 2001;533(Pt 1):15–22. https://doi.org/10.1111/j.1469-7793.2001.0015b.x PMID: 11351008

146. Fong AJ, Cai LL, Otoshi CK, Reinkensmeyer DJ, Burdick JW, Roy RR, et al. Spinal cord-transected mice learn to step in response to quipazine treatment and robotic training. J Neurosci. 2005;25(50):11738–47. https://doi.org/10.1523/JNEUROSCI.1523-05.2005 PMID: 16354932

147. Cai LL, Fong AJ, Otoshi CK, Liang Y, Burdick JW, Roy RR, et al. Implications of assist-as-needed robotic step training after a complete spinal cord injury on intrinsic strategies of motor learning. J Neurosci. 2006;26(41):10564–8. https://doi.org/10.1523/JNEUROSCI.2266-06.2006 PMID: 17035542

148. Sakurai A, Tamvacakis AN, Katz PS. Recruitment of polysynaptic connections underlies functional recovery of a neural circuit after lesion. eNeuro. 2016;3(4):ENEURO.0056-16.2016. https://doi.org/10.1523/ENEURO.0056-16.2016 PMID: 27570828

149. Rossignol S, Dubuc R, Gossard J-P. Dynamic sensorimotor interactions in locomotion. Physiol Rev. 2006;86(1):89–154. https://doi.org/10.1152/physrev.00028.2005 PMID: 16371596

150. Hicks AL, Ginis KAM. Treadmill training after spinal cord injury: it's not just about the walking. J Rehabil Res Dev. 2008;45(2):241–8. https://doi.org/10.1682/jrrd.2007.02.0022 PMID: 18566942

151. Nam KY, Kim HJ, Kwon BS, Park J-W, Lee HJ, Yoo A. Robot-assisted gait training (Lokomat) improves walking function and activity in people with spinal cord injury: a systematic review. J Neuroeng Rehabil. 2017;14(1):24. https://doi.org/10.1186/s12984-017-0232-3 PMID: 28330471

152. Feldman AG, Levin MF, Garofolini A, Piscitelli D, Zhang L. Central pattern generator and human locomotion in the context of referent control of motor actions. Clin Neurophysiol. 2021;132(11):2870–89. https://doi.org/10.1016/j.clinph.2021.08.016 PMID: 34628342

153. de Leon RD, Reinkensmeyer DJ, Timoszyk WK, London NJ, Roy RR, Edgerton VR. Use of robotics in assessing the adaptive capacity of the rat lumbar spinal cord. Prog Brain Res. 2002;137:141–9. https://doi.org/10.1016/s0079-6123(02)37013-4 PMID: 12440365

154. Cantoria MJ, See PA, Singh H, de Leon RD. Adaptations in glutamate and glycine content within the lumbar spinal cord are associated with the generation of novel gait patterns in rats following neonatal spinal cord transection. J Neurosci. 2011;31(50):18598–605. https://doi.org/10.1523/JNEUROSCI.3499-11.2011 PMID: 22171058

155. Pizzolato C, Gunduz MA, Palipana D, Wu J, Grant G, Hall S, et al. Non-invasive approaches to functional recovery after spinal cord injury: Therapeutic targets and multimodal device interventions. Exp Neurol. 2021;339:113612. https://doi.org/10.1016/j.expneurol.2021.113612 PMID: 33453213

156. Cabaj AM, Majczyński H, Couto E, Gardiner PF, Stecina K, Sławińska U, et al. Serotonin controls initiation of locomotion and afferent modulation of coordination via 5-HT7 receptors in adult rats. J Physiol. 2017;595(1):301–20. https://doi.org/10.1113/JP272271 PMID: 27393215

157. Danner SM, Zhang H, Shevtsova NA, Borowska-Fielding J, Deska-Gauthier D, Rybak IA, et al. Spinal V3 interneurons and left-right coordination in mammalian locomotion. Front Cell Neurosci. 2019;13:516. https://doi.org/10.3389/fncel.2019.00516 PMID: 31824266

158. Rybak IA, Dougherty KJ, Shevtsova NA. Organization of the Mammalian locomotor CPG: review of computational model and circuit architectures based on genetically identified spinal interneurons (1,2,3). eNeuro. 2015;2(5):ENEURO.0069-15.2015. https://doi.org/10.1523/ENEURO.0069-15.2015 PMID: 26478909

159. Feng J. Is the integrate-and-fire model good enough?–a review. Neural Netw. 2001;14(6–7):955–75. https://doi.org/10.1016/s0893-6080(01)00074-0 PMID: 11665785

160. Merzon L, Malevich T, Zhulikov G, Krasovskaya S, MacInnes WJ. Temporal limitations of the standard leaky integrate and fire model. Brain Sci. 2019;10(1):16. https://doi.org/10.3390/brainsci10010016 PMID: 31892197

161. Edlund JA. Numerical investigation of spinal neuron facilitation with multi-electrode epidural stimulation. California Institute of Technology; 2019.

162. Lavrov I, Dy CJ, Fong AJ, Gerasimenko Y, Courtine G, Zhong H, et al. Epidural stimulation induced modulation of spinal locomotor networks in adult spinal rats. J Neurosci. 2008;28(23):6022–9. https://doi.org/10.1523/JNEUROSCI.0080-08.2008 PMID: 18524907

163. Jung Y, Breitbart S, Malvea A, Bhatia A, Ibrahim GM, Gorodetsky C. Epidural spinal cord stimulation for spasticity: a systematic review of the literature. World Neurosurg. 2024;183:227-238.e5. https://doi.org/10.1016/j.wneu.2023.12.158 PMID: 38181878

164. Parker J, Dietz BE. Spinal cord stimulation for the relief of spasticity from cerebral palsy. Healthcare Tech Letters. 2020;7(3):93–7. https://doi.org/10.1049/htl.2019.0109

165. Elbasiouny SM, Moroz D, Bakr MM, Mushahwar VK. Management of spasticity after spinal cord injury: current techniques and future directions. Neurorehabil Neural Repair. 2010;24(1):23–33. https://doi.org/10.1177/1545968309343213 PMID: 19723923

166. Brzosko Z, Mierau SB, Paulsen O. Neuromodulation of spike-timing-dependent plasticity: past, present, and future. Neuron. 2019;103(4):563–81. https://doi.org/10.1016/j.neuron.2019.05.041 PMID: 31437453

167. Caron G, Bilchak JN, Côté M-P. Direct evidence for decreased presynaptic inhibition evoked by PBSt group I muscle afferents after chronic SCI and recovery with step-training in rats. J Physiol. 2020;598(20):4621–42. https://doi.org/10.1113/JP280070 PMID: 32721039